ANALYSIS OF THE REDUCTION KINETICS OF A FISCHER-TROPSCH Co/TiO_2 CATALYST USING TEMPERATURE PROGRAMMED REDUCTION: THE IMPLICATIONS AND APPLICATIONS TO INDUSTRY

Mukuka S. Bowa Chansongo

A dissertation submitted to the Faculty of Engineering and Built Environment, University of the Witwatersrand, Johannesburg, in fulfillment of the requirements for the degree of Master of Science.

Johannesburg, 2009.

DECLARATION

I declare that the dissertation is my own, unaided work. It is being submitted for the Degree of Master of Science in the University of the Witwatersrand, Johannesburg. It has not been submitted before for any degree or examination in any other University.

_____

(Signature)

_____ day of _____ 20 _____

ABSTRACT

Reduction is a critical step in catalyst preparation in chemical processes. Stability, activity and selectivity of catalysts are affected when certain parameters, such as temperature and water partial pressures, are not controlled during reduction.

The main objective of this work is to use information from Temperature Programmed Reduction (TPR) that is both quantitative and qualitative, based on the existing literature, experimental data, and the researcher's assumptions, to understand the implications of the reduction conditions on catalyst in an industrial fixed-bed reactor. This investigation has been carried out using simple mass balance calculations; evaluating reduction parameters; developing and applying methods of kinetic analysis and modeling, for a better comparative insight into real operating conditions.

A Co/TiO_2 catalyst used in Fischer-Tropsch (FT) synthesis of hydrocarbons from syngas generated by reforming natural gas and/or coal has been used to illustrate this analysis. The catalyst was prepared by incipient wetness.

To obtain accurate results for kinetic analysis, a custom-built TPR was modified and optimized. The parameters used in the analysis to determine the position of the maximum rate and shape of H_2 consumption peaks were also optimized.

Simple mass balance calculations were made on TPR system to determine the rate of reduction and P_{H_2O} during the process. This information (and relevant literature on the subject) was used to evaluate the implications P_{H_2O} on catalyst reducibility in a 12m long tube.

To evaluate the effect of different parameters on catalyst reducibility, flow rate, ramping rate, catalyst grain size and drying time prior to reduction were studied. It was found that heating rate and drying time prior to reduction had a significant impact on catalyst reducibility.

It has been established that a lower ramping rate maximizes the extent of reduction to active Co metal at low temperatures, while at the same time ensuring an equilibrium particle size which is stable against sintering.

The study of the effect of water content in the catalyst prior to reduction led to the conclusion that it has a significant effect on catalyst reducibility. However, to arrive at a more conclusive explanation of the effect it was recommended that further FT experiments should be performed on the catalyst with varying amounts of water content to investigate the effect, not only on the reducibility but also the activity and selectivity of the catalyst.

It has been shown that kinetic analysis using TPR can be used to determine the optimum reduction temperature among those that occur at different stages (in the case of multi-step reduction). These can then be used to predict the amount of H_2 that will be consumed with increasing temperatures.

Furthermore, this study has established that the mechanism of reduction obtained from kinetic analysis can help understand the degree of reduction observed at various temperatures. It can also contribute to an explanation of the stages of reduction and underlying gas-solid reactions, which in turn make it useful as a guide to monitor and control P_{H_2} throughout the reduction process in a 12m long tube.

ACKNOWLEDGEMENTS

Thanks be to God, the most high.

My sincere gratitude is owed to my supervisors Professor David Glasser and Professor Diane Hildebrandt, for their support, guidance and warmth. It has been a great privilege to work under their care.

Thanks are also due to: Dr Kalala Jalama and Dr Liu for their assistance; Basil Chassoulas and Victor Msimangu for technical support in the lab; and my colleagues and the staff at COMPS, for making my study worthwhile.

To my friends in Room 310 Thierry, Kutemba, Julie, Yali, Kalala, Alex, Cornellius and Mr Tabrizi, I sincerely appreciate your friendship.

My husband Fred and son Samuel deserve special thanks for their love and support, as does my dad, who has always believed in me.

I must also acknowledge the financial support provided by the Centre of Materials and Process Synthesis (COMPS), the National Research Foundation (NRF), the Postgraduate Merit Award (PMA) and the University of the Witwatersrand.

CONTENTS

CHAPTER 5 KINETIC MODELLING OF TPR ANALYSIS

CHAPTER 6 CONCLUSIONS AND RECOMMENDATIONS

LIST OF FIGURES

CHAPTER 2

CHAPTER 3

CHAPTER 4

CHAPTER 5

APPENDIX 1

APPENDIX 2

APPENDIX 5

APPENDIX 6

LIST OF TABLES

CHAPTER 2

CHAPTER 3

CHAPTER 4

CHAPTER 5

APPENDIX 2

APPENDIX 4

APPENDIX 5

APPENDIX 6

LIST OF SYMBOLS AND ABBREVIATIONS

A : pre-exponential factor

E_a : Activation energy (Jol mol^{-l})

f (α) : Reaction model

FT : Fischer-Tropsch

Gpf : Gaussian Probability Function

P : Pressure (bar)

PID : Proportional integral derivative controller

R : Gas constant (J/mol.K)

Syngas: mixture of CO and H_2

T : Absolute temperature (Kelvin, K)

TG : Thermogravimetry

TPR : Temperature Programmed Reduction

∆G : Gibbs free energy

A : Degree of reduction

π (x) : approximation of the temperature integral

CHAPTER 1

INTRODUCTION

Some catalytic reactions in chemical processes do not work as well as expected because of low catalyst activity. This may be attributable to poor catalyst pretreatment procedures, which results in the use of more resources, either for regeneration or replacement of the catalyst. Understanding, selection and optimization of reduction procedures in reactors for oxide catalysts are all critical for producing catalysts of high activity, the desired selectivity and long life (high stability) that will support optimal product yields.

Reduction is a critical step in catalyst preparation. Improperly reduced catalysts (for example those reduced too rapidly or overheated) exhibit poor activity and selectivity. However, temperature is not the sole cause of these deficiencies: water partial pressure (P_{H_2O}) during reduction can also influence the properties of the catalyst. The exact mechanism affecting catalytic activity by virtue of P_{H_2O} effects is not clearly understood, but the effect is clearly recognizable in reduction of bulk catalysts, and in many cases can be irreversible.

To study the reduction behaviour of catalysts, Temperature Programmed Reduction (TPR) technique was used to obtain the reduction kinetics of Co/TiO_2. The resultant information was used to evaluate industrial applications and implications. The implications of reduction of catalyst in a TPR reactor for that of bulk catalysts were also made. In the case of an industrial reactor only one tube in a fixed bed reactor was considered and hereafter referred to it as a '12 m long tube'.

1.1 MOTIVATION

This dissertation is motivated by a dual purpose: to understand the reduction mechanisms and kinetics of Fischer-Tropsch (FT) metal oxide catalysts; and to develop a reduction model that can be used both in the investigation of water partial pressures during reduction and in the optimization of reduction procedures in industry.

The TPR technique, run under conditions that do not necessarily differ much from the real operating conditions of the catalyst, has been used to investigate the behaviour of a catalyst during reduction. Quantitative and qualitative information relating to TPR, which was based on experimental data, published literature and assumptions, was used to generate simple

reduction flow sheets. These provided a basis for the investigation of the water partial pressures to be expected in industry. A comparative study of catalyst behaviour was undertaken using TPR operated at two extremes (that is, the lowest and highest parameter values within the TPR-recommended range of conditions). Such an approach made it possible to offer a rapid evaluation of the behaviour of catalysts under different conditions, which made it easier to evaluate the implications that the information obtained would have for catalysts in a 12m long tube.

1.2 OBJECTIVES

This work aimed to use quantitative and qualitative information on TPR derived from the literature on the subject, experimental data, and assumptions to understand the implications of reduction conditions on catalysts in a 12m long tube in an industrial context. The objectives of the research were to evaluate reduction parameters, to develop and apply methods of kinetic analysis, and devise a reduction model. This would provide a better comparative understanding of real operating conditions and open the way for the design of better reduction procedures.

1.3 DISSERTATION OUTLINE AND SCOPE

The dissertation consists of six chapters.

Chapter 2 reviews the literature on reduction and the use of TPR in the reduction kinetic analysis of heterogeneous systems.

Chapter 3 describes the methodology used in the research, which includes catalyst preparation, TPR set-up, optimization of experimental conditions, TPR product evaluation and its application in a 12m long tube.

Chapter 4 presents a comparative study of catalyst behaviour under different conditions by using TPR operated at two extremes, in other words the lowest and highest parameter values within the TPR-recommended range of conditions. The parameters studied include flow rate, heating rate, particle diameter cuts and drying time prior to reduction.

Kinetic and mechanistic evaluation of Co/TiO_2 catalysts is presented in Chapter 5. The kinetic analysis is not based on accurate kinetic evaluation, but instead focuses on obtaining information that will help explain how the reduction rate is affected by temperature for different heating rates, and assessing the implications this will have on catalysts in a 12m long tube.

Conclusions and recommendations based on the objectives are discussed in Chapter 6.

CHAPTER 2

LITERATURE REVIEW

2.1 FISCHER-TROPSCH HETEROGENEOUS CATALYSTS

The Fischer-Tropsch (FT) process is a catalyzed chemical reaction in which synthesis gas (syngas), a mixture of CO and H_2, is converted into liquid hydrocarbons of various forms. The principal purpose of FT is to produce synthetic petroleum substitutes, typically from coal, natural gas or biomass, for use as a fuel and as a chemical feedstock.

Active commercial catalysts used in FT synthesis include Co, Fe, Ni (Fischer, F., 1931) and Ru (Pichler, H., 1940). Ru is scarce and hence too expensive. Ni catalysts have high activity but produce too much methane. Also, their performance at high pressure is poor, due to their production of volatile carbonyls (Anderson, R. B., 1984). This leaves only Co and Fe as practical choices of catalyst. Co has the advantage of higher activity and longer life, though on a metal basis it is 1 000 times more expensive than Fe.

2.2 CATALYST REDUCTION

Prior to FT synthesis, a catalyst precursor is subjected to reduction, the purpose of which is to bring the catalyst into an active form for synthesis. Co, Ni and Ru are almost always reduced in flowing H_2 to the zero-valent metallic state, in which they remain during synthesis, under a variety of conditions (Anderson, R. B., 1956). Other gases such as carbon monoxide and syngas are also used as reduction agents.

Reduction is an important step in catalyst preparation, because their activity and selectivity are affected when certain parameters such as temperature and P_{H_2O} are not controlled during reduction. Unsatisfactory effects resulting from lack of control over the temperature appear to be reversible, whereas P_{H_2O} effects in most cases seem to be irreversible. In other words, incomplete reduction at relatively low temperatures or over-reduction at relatively high temperatures both lead to poor catalytic activity, which can be remedied and catalyst activity restored (Yulong Zhang et al. (1999)).

Water partial pressures can be substantially reduced if both water and hydrogen partial pressures are controlled during reduction. This is practicable in a lab set-up, but it may prove impossible to exercise as much control over

the large amount of water produced at the outlet of a 12m long tube. Therefore other means of eliminating water may have to be considered. An investigation of the impact of water concentration on catalyst performance was investigated and it was discovered that the presence of water vapour during reduction can enhance the deactivation of cobalt catalysts through surface oxidation or the formation of a compound between the metal and support (Kogelbauer et al., 1996; Schanke et al., 1995).

Hydrocarbon synthesis catalysts are usually prepared by depositing a metal, such as cobalt or other Group VIII metals, onto a support. This is done by techniques such as impregnation (Richardson, J. T, 1989 and Acres et al., 1981), using metal in a water-soluble (such as cobalt nitrate) or hydrocarbon-soluble (for example cobalt carbonyl) form. The catalyst is usually dried to eliminate the solvent, but reduction does not occur during the drying step, even though a hydrogen-containing gas may be used as the drying agent, because drying is carried out at low temperatures. The drying of the catalyst prior to reduction is essential to remove water (Delmon et al, 2005).

Reduction to the elemental or catalytically active form of metal may proceed directly from the metal compound. Alternatively it may be converted to a more easily reducible form, such as oxide, and then reduced to its elemental or catalytically-active form.

The reduction of a metal oxide by a reducing agent (H_2, CO) can be summarized by equations 2.1 and 2.2.

$M_XO_Y + yH_2 \leftrightarrow yH_2O + X_m$……..….2.1.

$M_XO_Y + yCO \leftrightarrow yCO_2 + X_m$……..……2.2.

The general aims of a successful pre-treatment (reduction) are to obtain catalysts of high activity, the desired selectivity and long life (high stability).

2.3 CATALYST CHARACTERIZATION

The intention behind catalyst characterization is to determine the physical and chemical properties of metal oxides and relate them to their catalytic properties. Catalyst characterization provides important information about the structure of FT catalysts and their experimental precursors. It also allows identification of active sites for FT reaction, and suggests possible routes for optimization of catalyst structure. The emphasis is mainly on developing an active, selective and mechanically robust catalyst. In order to accomplish this, tools are needed that identify those structural properties that discriminate

Table 2.1: Important methods of characterization for FT catalysts

Abbreviation	*Technique*	*information acquired*
BET	Brueller–Emmett–Teller	Determination of pore diameter, distribution and volume
EXAFS	Extended X-ray absorption fine structure	Multi-metallic study
TEM	Transmission electron microscopy	Shape and morphology of metal particles
XRD	X-ray defraction	Powder pattern identification of crystalline phases
XPS	X-ray photoelectron spectroscopy	Identification of oxidized and reduced phases
TPx	Temperature Programmed reaction(x = Reduction, Oxidation, Desorption, Sulphidation or Surface Reaction)	Redox fingerprints of catalysts and detection of catalyst phases that are easy and difficult to reduce
Chemisorption	Chemisorption	Information about the number of active sites and evaluation of the extent of reduction
Electron Microscopy	Electron Microscopy	Identification of phases and structural information of crystals
TGA	Thermo-gravemetric Analysis	Measurement of the thermal stability and composition of a material

between efficient and less efficient catalysts. The wide range of physical and chemical techniques that have been used in the characterization of FT catalysts are summarized in Table 2.1(Khodakov et al, 2007).

2.4 TEMPERATURE-PROGRAMMED REACTION TECHNIQUES

Temperature-programmed reaction (TPR) techniques are characterization methods in which a chemical reaction is monitored by analyzing the gas composition of the reactor outlet, while the temperature increases in linear relation to duration (Falconer et al., 1983 and Barin et al., 1973).

Among thermoanalytical techniques, the most frequently-used for characterizing heterogeneous catalysts are temperature-programmed desorption (TPD) and temperature–programmed reduction (TPR). In TPD analysis, which was first reported by Amenomiya and Cvetanovic (1963), a solid is equilibrated with an adsorbing gas and then submitted to a programmed temperature rise while the amount of desorbing gas is continuously monitored.

Since then temperature-programmed techniques have been extended to cover oxidation, sulphidation, methanation, hydrogenation, gasification,

carburization and other catalytic surface reactions (TPO, TPS, TPM, TPH, TPG, TPC and TPSR respectively) (Kanervo J., 2003).

2.5 TEMPERATURE-PROGRAMMED REDUCTION (TPR)

TPR technique was first proposed by Robertson et al. (1985). In general, it is used to provide information on the effects of support materials, preparation and pretreatment procedures and metal additives on catalyst reducibility. Mass balance calculations and kinetic information obtained from TPR can be used in fundamental measurement of $\mathrm{P_{H_2}}$ and $\mathrm{P_{H_2O}}$, which have to be closely monitored and are critical during the reduction of bulk industrial catalysts. This technique can also be used quantitatively to determine the number of reducible species in the catalyst and the extent of their reduction from the consumption of hydrogen. Thus, it can be applied to mimic catalyst reduction in a 12m long tube and obtain an advanced estimate of both the degree and the temperature of reduction. Further, the shape and position of reduction peaks can supply information about the degree of interaction between the oxidic precursor and the support which is vital in catalyst development.

In TPR a reducible precursor is exposed to the flow of a reducing gas mixture (typically nitrogen or argon containing a few volume percent of H_2, CO or

syngas), while the temperature is increased on a linear scale. The rate of reduction is continuously charted by measuring the composition of the reducing gas mixture at the outlet of the reactor. The experiment permits the evaluation of the total amount of reducing gas consumed, from which the degree of reduction, and thus the average oxidation state of the solid material after reduction, can be calculated.

TPR can be modified to study the effect of water on the reducibility of a catalyst during reduction, and thus provide guidance on the P_{H_2O} effects on catalysts to be expected in a 12m long tube. In earlier work done by Yulong Zhang et al. (1999), TPR was used to investigate the effect of water vapour on the reduction of Ru-promoted Co/Al_2O_3 by introducing water vapour during a standard reduction procedure. It was observed that the addition of up to 3% water vapour during standard reduction resulted in a decrease in the amount of reducible Co from 92 to 45%. Zhang and his colleagues concluded that the decrease in the degree of reduction of Co was due to interaction between CoO with the support, and the formation of non-reducible species.

TPR has also been extensively used to determine the rates and kinetics of reduction. Kissinger, H. E. (1957) developed a method to determine activation values from differential thermal analysis (DTA) patterns by measuring the displacement of the DTA peak maximum as a function of the heating rate.

Wimmers et al. (1986) later applied the Kissinger analysis to TPR by using various kinetic models. Tafaoui (1996) based another method on multiple heating rates and applied to TPR studies. This technique (which was originally published by Friedman, H. L. in 1963) yields more information than Kissinger's approach, since it provides apparent activation energy estimates for different reduction conversions.

Munteanu et al. (2008) observed that errors increase significantly if the recommendations by Monti and Baiker (1983) concerning choosing reduction parameters such as flow rate of the reducing gas, concentration of the H_2 and the amount of sample to be reduced are not followed. Other, more recent work by Rotaru et al. (2008), addresses errors encountered when using TPR to determine kinetic parameters, which indicate that discrimination procedures such as the invariant kinetic parameters (IKP) method (Lesnikovich and Levchick, 1983) and the Perez-Maqueda et al. (2002) criterion can be used only if activation energy (E_a) is independent of conversion. Furthermore the Rotaru publication notes that kinetic parameters are significantly dependant on heating rate, and that using the IKP approach, which involves "master plots" and use of derivative curves, can give rise to significant errors.

Qualitatively, TPR patterns contain information on the nature of the reduction process. In favourable cases where the catalyst particles are uniform, TPR yields both kinetic and mechanistic information which has been widely described and reviewed (Lin and Chen, 2004; Wan et al., 2007; Hurst et al., 1982; Monti and Baiker, 1983; Malet and Caballero, 1988; Knözinger, H., 1997; Wimmers et al., 1985; Kissinger, H. E., 1957; Munteanu et al., 2008; and Adventovic and Jankovic, 2008).

Despite the extensive study of TPR kinetic analysis and the amount of qualitative and quantitative information obtained by these means, the implications of these findings have rarely been extended to large-scale or commercial operations.

In the research carried out for this dissertation, TPR has been used to explain how reduction is influenced by the choice of parameters, and the implications this may have both in a specific context (a 12m long reactor tube in industry) as well as in a more general application, like the design of better reduction procedures commercially.

2.6 THE THERMODYNAMICS OF REDUCTION

Consider the reduction of a metal oxide MO_X by H_2 as shown in equation 2.3.

$$MO_X + XH_2 \leftrightarrow M + X\,H_2O \quad \text{.....2.3.}$$

Thermodynamics predicts under which conditions a catalyst can be reduced. As with every reaction, the reduction will be favorable when the change in Gibbs free energy (ΔG) has a negative value.

Equation 2.4 shows how ΔG depends on pressure, composition and temperature.

$$\Delta G = \Delta G^o + nRT \ln \left[P_{H_2O} / P_{H_2} \right] \quad \text{.....2.4.}$$

where ΔG is the change in Gibbs free energy for the reduction (Joules), n the stoichiometric coefficient of reaction, T the temperature (Kelvin), R the universal gas constant (8.314 m^3 Pa/ mol K), and P_i the partial pressure of component i (Pa), for instance H_2 and H_2O.

If the catalyst is reduced under the flow of hydrogen, the reaction product (water) is removed effectively and the second term in equation 2.4 is therefore always negative.

For many metals such as Co, Ni and noble metals, ΔG^{o} is already negative and reduction is thermodynamically permitted. All that needs to be done is to find a temperature at which the rate is rapid enough to achieve complete reduction.

In order to see whether reduction is thermodynamically permitted, equation (2.4) is written as:

$$\Delta G = nRT\ ln[(\frac{P_{H_2O}}{P_{H_2}})/(\frac{P_{H_2O}}{P_{H_2}})_{eq}] \quad \text{.....2.5,}$$

with the symbols as above, and the subscript ‘eq’ for equilibrium ratio.Thus ΔG is negative when the ratio P_{H_2O}/P_{H_2} is smaller than the equilibrium value.

2.7 MECHANISMS OF REDUCTION

2.7.1 Metal oxides

The process by which a sphere metal oxide is reduced directly to a metal, in a stream containing hydrogen under isothermal conditions, has been considered. The degree of reduction, α, observed as a function of time, t, for various temperatures and pressures of $H_{2,}$ constitutes the kinetics of reduction, which are interpreted in terms the mechanism through which reduction occurs. This has been interpreted in terms of the contracting sphere and nucleation models.

The shrinking core or contracting sphere model

In the shrinking core model the dissociation of $H_{2,}$ in the initial step occurs very swiftly, as may be observed on noble metal oxides or highly defective oxide surfaces. The essence of this model is that the nuclei of the reduced metal form rapidly over the entire surface of the particle, and grow into the shell of reduced metal. The movement of lattice oxygen out of the particle limits further reduction. The rate of reduction increases rapidly at first, but slows down as the metal shell grows.

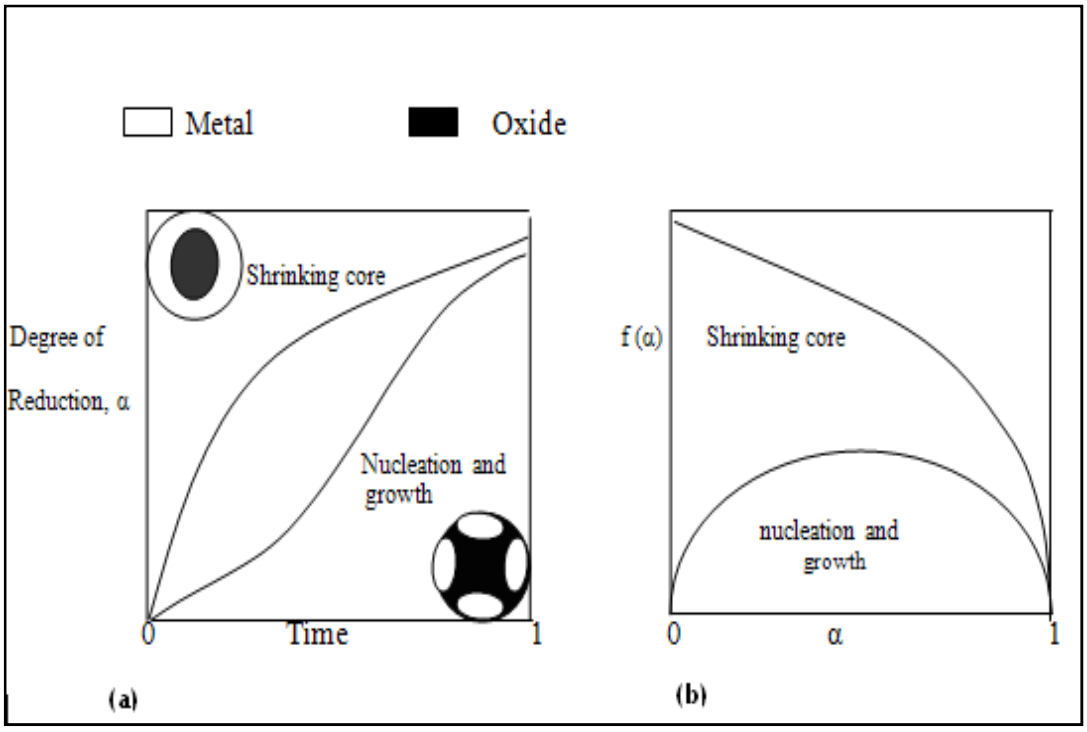

Figure 2.1 *Shrinking core and contracting sphere models (a) effect of the degree of reduction (α) on time (b) the effect of the reaction model (f (α)) on the degree of reduction (Niemantsverdriet, J. W., 1995).*

The nucleation model

In the contracting sphere model, the metal/metal oxide interface is continually decreasing, which results in the curved α against t plot illustrated in Figure 2.1 (a), and a continually decreasing reaction model (f (α)) throughout the reaction shown in Figure 2.1 (b).

When the oxide and hydrogen come into contact, the reaction starts. After some time, the first nuclei of the solid product form. Oxygen ions are removed from the lattice by reduction, and when the concentration of the vacancies reaches a certain critical value, they are annihilated by the rearrangement of the lattice and the eventual formation of metal nuclei.

The reaction interface, which may be visualized as the interaction between the nuclei of the metal and metal oxide, begins to increase more and more rapidly by two processes: the growth of the nuclei already formed; and the appearance of new ones. Oxygen may be removed by inward diffusion of hydrogen to the metal/metal oxide interface, or by outward diffusion of oxygen ions from the metal oxide to the metal/gas interface. At a certain stage of the reduction, the metal nuclei have grown on the surface of the oxide grains to such an extent that they begin to make contact with one another. This moment marks the beginning of a decrease in the reaction interface which results in the growth of the metal nuclei and the steady consumption of the oxide grains.

These processes continue until the oxide is completely reduced to the metal. The final stage, in which the reaction interface is shrinking as the metal layer grows, is equivalent to the contracting (or shrinking) sphere model. Figure 2.1

illustrates this nucleation mechanism, which results in the sigmoid-shaped α - against - t plot shown, and the maximum in the dα/dt - against - α plot.

2.7.2 Supported oxides

Reduction may be hindered or promoted, depending on the nature of the oxide/support interaction. Supported metal oxides may be homogeneously distributed across the surface of the support, or exist as islands of oxide separated by uncovered support. The latter may be expected to reduce in a manner similar to that of unsupported oxide, in which the support may act purely as a dispensing agent to promote the reduction. Under these conditions the reduction kinetics observed for supported oxide are of the same general form as those found for the bulk oxide.

More than 20 mechanistic functions have been reported in the literature on solid state transformations (Gao and Dollimore, 1993). Table 2.2 and Table 2.3 give f (α) functions for some gas–solid reaction models. The expressions are grouped according to the shape of the isothermal α- time curves as acceleratory, sigmoid or deceleratory. The deceleratory group is further subdivided according to whether the controlling factor assumed in the derivation is of the geometrical, diffusion or reaction order.

Table 2.2 Basic kinetic models for solid state transformation

Models	***Differential form f (α) =1/k d α/dt***	***Integral form g(α)= kt***
1. Acceleratory α-time		
Nucleation models		
Power law(P2)	$2\ \alpha^{(1/2)}$	$\alpha^{(1/2)}$
Power law(P3)	$3\ \alpha^{(2/3)}$	$\alpha^{(1/3)}$
Power law(P4)	$4\ \alpha^{(3/4)}$	$\alpha^{(1/2)}$
2. Sigmoid α-time		
Avraami-Erofeyev (A2)	$2(1-\alpha)\ [-\ln(1-\alpha)]^{1/2}$	$[-\ln(1-\alpha)]^{1/2}$
Avraami-Erofeyev (A3)	$3\ (1-\alpha)\ [-\ln(1-\alpha)]^{2/3}$	$[-\ln(1-\alpha)]^{1/3}$
Avraami-Erofeyev (A4)	$4(1-\alpha)\ [-\ln(1-\alpha)]^{3/4}$	$[-\ln(1-\alpha)]^{1/4}$
3. *Deceleratory*		
3.1 Geometric contraction models		
Contracting area(C2)	$2(1-\alpha)^{1/2}$	$[1-(1-\alpha)^{1/2}$
Contracting area(C3)	$3(1-\alpha)^{1/3}$	$[1-(1-\alpha)1^{/3}]$
3.2 Diffusion models		
1-D DIffusion	$(1-\alpha)^{1/3}$	α^2
2D- diffusion	$1/[-\ln(1-\alpha)]$	$[(1-\alpha)\ln(1-\alpha)]+\alpha$
3-D Diffusion Jander	$3/2\ (1-\alpha)^{2/3}/[1-(1-\alpha)^{2/3}]$	$[1-(1-\alpha)^{1/3}]$
Ginstling –Brounshtein	$3/2\ [(1-\alpha)^{-1/3}-1]$	$1-(2\alpha/3)-(1-\alpha)^{2/3}$
3.3 Reaction order models		
Zero-order	1	α
First order	(1- α)	Ln(1- α)
Second order	$(1-\alpha)^2$	$(1-\alpha)^{-1}-1$
Second order	$(1-\alpha)^3$	$½[(1-\alpha)^{-2}-1]$

The f (α) function varies with different reaction models. Sesták (1984) proposed the term “accommodation coefficient” for any terms other than (1-α), which are needed to modify equations based on reaction order for application to heterogeneous systems.

This is often referred to as the Sesták- Berggren (SB) equation, which is expressed as:

$$\frac{d\alpha}{dt} = K\alpha^{n}(1-\alpha)^{n} \quad \text{.....2.6.}$$

Unlike the Avraami–Erofeev model, which is based on ideal conditions, the SB model is flexible and can be used for quantitative description of complex processes.

In addition to the basic kinetic models that correspond to certain geometries of the reaction interface, there are also empirical kinetic models, as shown in Table 2.3, which demonstrate that acceptable values of the parameter m for SB models are confined to the interval 0<m<1 (Malek, J., 1989).

Table 2.3 Empirical kinetic models

Models	*Symbol*	*f (α)*
Reaction order	RO (n)	$(1-\alpha)^n$
Šesták-Berggren	SB (m,n)	$\alpha^m (1-\alpha)^n$

2.8 KINETICS OF TPR

TPR has not been limited to surface characterization. It has also been used in the study of kinetics of solid state reactions for the determination of activation energy, E_a; the reaction model, f (α); and the pre-exponential factor, A. In earlier kinetic research on silica-supported cobalt conducted by Lin and Chen (2007) using TPR, the evaluation of kinetic parameters is based on the assumption that the maximum rate of reaction occurs at the peak maximum of the TPR pattern, and does not change with heating rate. The values of E_a and A are thus obtained from experimental data at the maximum point of TPR using different heating rates. In this way simulated TPR patterns are obtained from each kinetic model, and the best fit model selected. Wan et al used TG curves interactively with TPR profiles to evaluate E_a, A and linear correlation coefficients (R) for Co_3O_4/SiO_2 catalysts, and then checked the values by the

Achar (Achar B. N., 1969) and Coats and Redfern (1965) methods. Both studies on the reduction Co confirmed a two-step reduction for the first and second peaks. These were described as the Avraami nucleation and rate order models respectively.

The variations in activation energies that have been calculated in previous research publications (for example Wan et al (2007) and Lin and Chen (2003)), compared with those covered in this dissertation can be attributed to the different methods used to determine activation energies. Nevertheless, the work reported on in this text focuses on understanding Co/TiO_2 catalyst behaviour and determining how the kinetic information it elicits can be applied to bulk catalysts. Furthermore the evaluation of the reduction model is not based on an attempt to derive accurate mechanistic functions, but rather on arriving at a general reduction mechanism that describes the behaviour of a Co/TiO_2 catalyst during reduction, and then relating the information to the behaviour of bulk catalysts.

Fitting reduction models to a two-step reduction reaction, as in the case of Co_3O_4, poses a challenge in TPR modeling, since the two reduction steps overlap. This makes it difficult to fit reduction models to TPR profiles. In this dissertation, an attempt was made to separate the two peaks and analyze them individually. This approach was found to yield more information and to

provide a good basis for kinetic evaluation of complex reduction reactions involving multi-step reduction processes.

In work previously published by other researchers, parameter estimation by model fitting was applied to first-order rate reactions using a differential reactor model (Ehrhard et al., 1985). The work of Monti and Baiker(1983), and Malet and Caballero(1988) in estimating kinetic parameters helped to establish a quantitative basis for TPR technique. Wimmers et al (1986) suggested the use of a wider set of gas-solid reaction mechanisms, and Tafaoui, A., (1996) reviewed models for describing the kinetics of gas-solid reactions in copper oxide, manganese oxide and aluminum- supported vanadium oxide.

Reduction principles

For a heterogeneous solid-gas reaction, the reduction of metal oxide MO_n by H_2 is described by equation 2.7.

$$MO_n + n\,H_2 \rightarrow M + nH_2O \qquad \text{2.7.}$$

The rate of reduction, r, can thus be expressed as a product of a temperature-dependent factor, K_{red} (T), and two other factors (based on reaction model, f (α), and f' (P_{H_2}, P_{H_2O})) is the gas phase concentration,

$$r = d\alpha/dt = K_{red}(T)\, f(\alpha)\, f'(P_{H_2}, P_{H_2O}) \quad \text{.....2.8.}$$

The term α is the degree of reduction, while f (α) describes the reduction mechanism, f' (P_{H_2}, P_{H_2O})) is the gas phase concentration and the partial pressures of the gases present during reduction (H_2 and H_2O) are denoted by P_{H_2} and P_{H_2O} respectively.

It is assumed hydrogen is in excess and thus gas phase-dependent term f' (P_{H_2} and P_{H_2O}) is approximately a constant. Using the fact that the temperature increases linearly in time, (dT = βdt). K_{red} can be replaced by the Arrhenius equation and the reaction rate expressed by a well-known general equation:

$$\beta \frac{d\alpha}{dt} A\, exp\left(\frac{-E_a}{RT}\right) f(\alpha) \quad \text{.....2.9.}$$

Activation energy (E_a), pre-exponential factor (A) and the reaction model f (α) describe the rate of reduction and are called the Kinetic Triplet.

2.8.1 Activation energy evaluation

Some simple methods exist for extracting activation energies from thermo-analytical data, for example Kissinger's means of evaluating activation energy from DTA data, which relates the temperatures of the rate maxima (T_{max}), obtained with different heating rates (β) to the activation energy (E_a).

$$ln\left(\frac{\beta}{T_{max}^2}\right) + ln\left(\frac{E_a}{RA}\right) = -\frac{E_a}{RT_{max}} + ln\left(-\frac{df(\alpha)}{d\alpha}\right)_{T=T_{max}} \quad \text{.....2.10.}$$

Thus, if the slope of $\ln(\beta/T_{max^2})$ versus $1/T_{max}$ results in a straight line, the slope of the line equals $-E_a/R$, provided that the last term of equation 2.10 is constant.

Kissinger's is a model-free method, as it does not require any model assumptions to calculate E_a. However, it does not calculate E_a values at progressive α values, but rather assumes a constant E_a. Like methods that assume a single E_a value, this technique cannot detect reaction complexities (Vyazovkin and Wight, 1999).

.

There are other methods, in which activation energy is calculated at desired degrees of conversion. Friedman introduced the first of these for DTA patterns of polymer degradation, basing his method on transforming equation 2.9 by taking natural logarithms on both sides of the equation.

$$ln\left(\beta\frac{d\alpha}{dT}\right) = ln\,(A(f(\alpha)) - \frac{E_a}{RT}\,)\text{.....}\quad\text{2.11.}$$

If the plot of ln (β dα/dT*)* versus 1/T results in a straight line at a selected conversion level, that is at α = constant for several heating rates, the slope of the line equals E_a/R at that conversion.

In practice, Friedman's method introduces large errors for small values of $\beta\frac{d\alpha}{dT}$, for instance near the outset and sometimes towards the end of the reaction. Using logarithms helps, but integrating ensures the greatest improvement because it automatically reduces the error contributions.

Some integral isoconversional methods are based on the following relations obtained from equation 2.9 through integration:

$$g(\alpha) = \frac{A}{\beta}\int_0^T [exp\,(-\frac{E_a}{RT})]dT \equiv \frac{AE_a}{\beta R}\;p(x)\frac{A}{\beta}\;I(E_a,T)\quad\text{.....2.12.}$$

where: $g(\alpha) \equiv \int_0^{\alpha} \frac{d\alpha}{f(\alpha)}, x = \frac{E_a}{RT}$ and p(x) is the temperature integral, which cannot be exactly calculated.

Flynn S. V., (1997) presented and critically discussed the various approximations suggested for the temperature integral. The isoconversional integral method suggested independently by Flynn and Wall (1966) and Ozawa (1965) uses Doyle's approximation of p (x) (Doyle C., 1962). This method is based on the equation:

$$ln\beta = ln\frac{AE_a}{R_G(\alpha)} - 5.331 - 1.052\ \frac{E_a}{RT} \quad \text{.....2.13.}$$

Thus, for α = const., the plot obtained from thermograms recorded at several heating rates should be a straight line the slope of which can be used to evaluate activation energy. For x < 20, Doyle's approximation leads to errors higher than 10%. In such cases, Flynn (1983) suggested corrections that would obtain an accurate value for the activation energy.

The Kissinger–Akahira–Sunose (KAS) method (Kissinger, 1957 and Akahira and Sunose, 1971) is based on the Coats–Redfern approximation (Coats and Redfern, 1964), according to which, for 20 < x < 50:

$$p(x) \cong \frac{exp\,(-x)}{x^2}$$ ……..…….2.14.

An example of a more exact approximation of the temperature integral is suggested by Agrawal (1992). From relationships (2.13) and (2.14) it follows that:

$$ln\frac{\beta}{T^2} = ln\frac{AR}{E_a\, g(\alpha)} - \frac{E_a}{RT}$$ ……..…….2.15.

Thus, for α = const., the plot ln β/T^2 vs. (1/*T*) should be a straight line, the slope of which can be used to evaluate the activation energy.

The commonly-used methods for calculating activation energy are summarized in Table 2.4.

When determining kinetic parameters for activation energy using TPR data, the errors most frequently encountered by the researcher are caused by the unanticipated effects of experimental parameters like flow rate, hydrogen concentration in the reducing gas mixture or the mass of the sample, which influence the position and shape (Munteanu et al, 2008). In the same vein, Munteanu et al showed that using conventional isoconversion methods such as those of Kissinger or Coates and Redfern leads to an artificial dependence on conversion of activation energy. They also proposed that the Friedman

method can be used to determine the activation energy parameter from TPR data only when the findings of Monti and Baiker (1983) regarding the correlation between the mass of the oxide, the flowrate and H_2 concentration in reducing gas mixture are taken into account.

Table 2.4 Classification of commonly-used methods for calculation of activation

Description	***Procedure***	***Best-known accurate techniques***
Maximum rate methods	plots of ln (T_{max}^2/β) versus $1/T_{max}$	Kissinger
Rate-isoconversion method	plots of ln ($d\alpha/dt$) versus 1/T	Friedman
p(x) - isoconversion integral method	plots of ln (β/T^2) versus 1/T plots ln (β) versus 1/T plots ln (β/T^2) versus 1/T	Kissinger-Akahira-Sunose; Flynn and Wall; Ozawa; Agrawal

In this work, Friedman's method has been used to obtain estimate activation energies since the recommendations of Monti and Baiker(1983) have been followed when choosing the kinetic parameters.

2.8.2 Kinetic model evaluation (f (α))

Málek's method

The kinetic model which best describes the set of thermal analysis data can be obtained after the activation energy has been calculated. The method proposed by Málek ((Málek, J., 1989) was used in this work to make a broad evaluation of the kinetic models that described the mechanism of the two-step reduction of Co/TiO_2 catalyst.

To evaluate the kinetic model, two special functions y (α) and z (α), obtained by transformation of experimental data, are defined (Málek, J., 1989; Criado et al, 1989).

$$y(\alpha) = (d\alpha/dt)\, exp\,(x) \quad \text{.....2.16,}$$

$$z(\alpha) = \pi(x)\,(d\alpha/dt)\,T/\beta \quad \text{.....2.17,}$$

where x = E/RT and π (x) is an approximation of the temperature integral. The rational expression of Senum and Yang (1977) is used to estimate π (x):

$$\pi\,(x) = \frac{x^3 + 18x^2 + 88x + 96}{x^4 + 20x^3 + 120x^2 + 240x + 120} \quad \text{.....2.18.}$$

The y (α) function is proportional to the f (α) function. Thus by plotting the y (α) dependence normalized within the (0, 1) interval, the shape of the function f (α) is obtained. The y (α) function is therefore a diagnostic tool for kinetic model determination. The maximum alpha α_m for the y (α) and α^{∞}_p for the z (α) function are used to guide the choice of a kinetic model (Málek, J., 1989).

The criteria used in choosing the reduction model based on Málek's method are described in greater detail in Appendix 4.

2.8.3 Pre-exponential factor (A) evaluation

Knowing the value of the activation energy and the kinetic model, the pre-exponential factor is calculated using Málek's equation (1989):

$$A = \frac{\beta x_p}{T f'(\alpha_p)} exp\; x_p \quad \text{.....2.19,}$$

where f'(α) is the differential form of the kinetic model, α_p is the degree of conversion corresponding to the maximum on the differential rate heating rates of TPR profiles.

Reports in various publications have demonstrated that TPR can be reliably used to study heterogeneous systems of reduction kinetics, and that it can be modified to examine the effect of P_{H_2O} on the reducibility and activity of Co catalysts. TPR is valuable because it can provide catalyst characterization of a chemical nature under conditions that are similar to real operating conditions in which the catalyst is used.

The interpretation of TPR is usually confined to a discussion of rate, maximum temperatures, the number of more or less resolved peaks or determination of the total consumption of reactant or evolution of product. However, in the case of this research, TPR is used to study the reduction kinetics of a Co/TiO_2 catalyst and to analyze the implications of the information gained for catalysts in a 12m long tube. It will also look at ways in which the data can be applied in the design of more effective reduction procedures.

2.9 REFERENCES

1. Achar, B. N. (1969) *Proceedings of the International* Clay Conference*.,*16
2. Acres, G. J. J., Bird, A. J., Jenkins, J. W. and King, F. (1981), *Catalysis-Special Periodicine Reports*, 4, 2.
3. Agrawal, P. K. (1992), *Thermochim. Acta*, 203, 93
4. Amenomiya, Y. and Cvetanović, R. J. (1963), *Journal of Physical Chemistry*, 67, 270 –2708.
5. Akahira, T. and Sunose, T. (1971), *Research Report Chiba Institute of Technology*., 16 22
6. Anderson, R. B. (1956), *Van Nostrand Reinhold*, New York, volume 4.
7. Armouldy, P. and Moulijn, J. A. (1985), *Journal of Catalysis*, 93, 38.
8. Avrami, M. (1940), *Journal of Chemical Physics*, 8, 212–224.
9. Coats, A. W. and Redfern, J. P. (1964) *Nature*, 68, 201.
10. Cvetanovic, R. J. and Amenomiya, Y. (1963), *Journal of Physical Chemistry*, 67, 2705 - 2708.
11. Delmon,D., Jacobs, P.A,Maggi, R.,Martens, J.A.,Grange, P. and G.Poncelet,2005,*Proceedings of the 7th international symposium,* Elsevier Science, Amsterdam, The Netherlands.
12. Doyle C. (1962), *Journal of Polymer Science,* 6, 639.

13. Ehrhard, K., Richter, M. R. and Ohlman, G. (1985), *Applied Catalysis*, 17, 23-45.
14. Falconer, J. L, and Schwarz, J. A. (1983), *Catalysis Reviews*, 25, 141 – 227.
15. Fischer, F. and Meyer, K. (1931), Brennstoff-Chemistry, 12, 225
16. Flynn, J. H. (1997), *Thermochim. Acta*, 300, 83–92.
17. Flynn, J. H. (1983), *Journal of Thermal Analysis,* 27, 95.
18. Flynn S. V. (1997), *Journal of Thermal Analysis*, 49 1493
19. Flynn J. H. and Wall L. A. (1966), *Journal of Physical Chemistry*., 70A, 487
20. Friedman, H. L. (1963), *Journal of Polymer science,* Part C 6, 183–195.
21. Gao, X. and Dollimore, D. (1993), *Thermochimica Acta*, 215, 47-63.
22. Lin, H. Y. and Chen, Y.W. (2003), *Thermochimica Acta*, 400, 61-67.
23. Lin, H.Y. and Chen, Y.W. (2004), *Materials Chemistry and physics* 851, 71-175.
24. Hurst, N. W., Gentry, S. J., Jones, A. and McNicol, B. D. (1982), *Catalysis Reviews – Science and Engineering*, 24, 33.
25. Janković, B. A. and Mentus, S. (2007), *Thermochimica Acta*, 456, 48–55.
26. Khodakov A.Y., Chu W. and Fongerland P. (2007), *Chemistry Reviews*, 107, 169-1744.
27. Kapteijn, F., Moulijn, J. A. and Tarfaoui, A. (1999), *Studies in Surface Science Catalysis*, 123, 525-541.

28. Kissinger, H. E. (1957), *Analytical Chemistry*, 29, 1702–1706.
29. Knözinger, H., Ertl, G. and Weitkamp, J. (1997), *Handbook of Heterogeneous Catalysis*; Eds.; VCH.
30. Kogelbauer, A., Goodwin J.G. and Oukaci, R. (1996), *Journal of Catalysis,* 160, 125.
31. Kanervo Jaana, 2003, Helsinki University of Technology, Department of Chemical Technology, Espoo.
32. Lamitre J. L., and Dellannay, F. (1984), Marcel Dekker, Inc.New York, 29-70
33. Lesnikovich, I. and Levchik S.V. (1985), *Journal of Thermal Analysis and Calorimetry,* 30, 237.
34. Hurst, S. J., Lemaitre N. W, Gentry, A. and Mc Nicol, B. D. (1982), *Catalysis Reviews – Science and Engineering*, 24, 233.
35. Malet, P. and Caballero A. (1988), *Journal of the Chemical Society*, *Faraday Transactions*, 84, 2369-2375.
36. Málek, J. (1992), *Thermochimica Acta*, 200, 257–269.
37. Monti, D. A. M. and Baiker, A. (1983), *Journal of Catalysis*, 83, 323-335.
38. Munteanu, G., Miclea, C., and Segal, E. (2008) Journal of *Thermal Analysis and Calorimetry,* 94, 317-321.
39. Niemantsverdriet J. W., *Spectroscopy in Catalysis: An Introduction*, Edittion 3, 2007, Eindhoven University of Technology, the Netherlands.
40. Ozawa T., (1965), *Bulletin of the Chemical Society of Japan*, 38, 1881

41. Perez-Maqueda, Criado, J. M., Gotor, F.G. and Malek, J. (1983), *Journal of Physical Chemistry,* 27, 89.
42. Pichler H., Frankenburg W., Rideal E. and Komarewsky V., (1952), *Advances in Catalysis*, vol. IV, Academic Press, New York, 271.
43. Richardson J.T. (1989), *Principles of Catalyst Development*, plenum press 111-112
44. Robertson S., McNicol B.D, Baas J.H, Kloet S.C and Jenkins J.W. (1975), *Journal of Catalysis,* 37, 424.
45. Rotaru, A., Goşa, M. and Rotaru, P. (2008), *Journal of Thermal Analysis and Calorimetry,* 94, 367-371.
46. Schanke, D., Hilmen, A. M., Bergene, E., Kinnari K., Rytter E., Adnnanes, E. and Holmen, A. (1995) *Catalysis letters*, 34, 269.
47. Sexton, B.A., Hughes, A.E. and Turrney, T.W. (1986), *Journal of catalysis*, 97, 390.
48. Senum, G. I and Yang, R. T. (1977), *Journal of Thermal Analysis*, 11, 445
49. Sestek, J. (1984), *Thermophysical Properties of Solids, Their Measurement and Theoretical Analysis*, Elsevier, Amsterdam,
50. Sestak, J., Satava, V. and Wendlandt, W. W. (1973), *Thermochim. Acta*, 7, 333-556.
51. Simon, J. (2004)*, Thermal Analytical Calorimetry*, 76, 123–132.
52. Sorai, M. (2004), *Comprehensive Handbook of Calorimetry and Thermal Analysis*, John Wiley and Sons, Inc., Chichester

53. Tafoui, A. (1996), Phd thesis, Delft University of Techchnology, The Netherlands.

54. Wu, Y-H., Wu, T., Chen, T., Weng, W. and Wan, H. (2007*), Materials Letters*, 61.

55. Vyazovkin, C. A. Wight: (1999), *Thermochim. Acta*, 341, 53–68.

56. Wan, J. Y., Li, L. J. and Chen, D. H. (2007*), Journal of Thermal Analysis and calorimetriy*, 90, 415 - 419.

57. Wimmers, O.J., Arnoldy, P. and Moulijn, J. A. (1985), *Journal of Physical Chemistry*, 89, 4517.

58. Wimmers, O.J, Arnoldy, P., and Moulijn, J.A. (1986), *Journal of Physical Chemistry*, 90, 1331-1337.

59. Yulong, Z., Dongguang, W., Sonia H. and Goodwin, J.G., (1999), *Journal of Catalysis*, 188, 281-290.

CHAPTER 3

EXPERIMENTAL

3.1 INTRODUCTION

The interpretation of TPR on a quantitative basis is fairly straightforward. However obtaining kinetic parameters such as activation energy or the pre-exponential factor is rather more complicated. TPR is very sensitive and easily affected by a number of factors such as flow rate, the amount of catalyst used in analysis, atmospheric pressure and the position of the reactor in the furnace. It is therefore important to bear them in mind in order to obtain reproducible experimental results.

This chapter describes the methodology used, which includes catalyst preparation, TPR set-up, TPR product evaluation (application for a 12m long tube) and optimization of the experimental conditions. The specific details of the TPR analysis procedure used will be described in the appropriate chapters.

3.2 CHEMICALS AND GASES

Different chemicals and gases were used in the TPR experiments and catalyst preparation.

3.2.1 Gases

Two gases, 99.99% Ar and 5% H_2/Ar, were used in the analysis. They were supplied by AFROX (African Oxygen) in cylinders, and certified as ultra-high quality (UHP). Argon was used for degassing and drying the catalyst prior to reduction, and 5% H_2/Ar mixture for the catalyst reduction.

3.2.2 Catalyst

A 10% cobalt on titania (10wt% Co_3O_4/TiO_2) catalyst prepared by a single-step incipient wetness impregnation of TiO_2 support with Co nitrate was used in the analysis.

Catalyst preparation

TiO_2 with surface area of $50m^2g^{-1}$ and pore volume of $0.35m^3g^{-1}$ was mixed with deionised water in a mass ratio of 1:1, and dried in air at 120°C for 1 hour. The support was calcined in air at 400°C for 16 hours. After calcination it was crushed and sieved to a particle size of 0.5-1 mm and used in the preparation of the catalyst.

The Co source was loaded onto TiO_2 as cobalt nitrate ($Co(NO_3)_2.6H_2O$) solution by the method described by Acres G.J.J. (1989). The catalyst was then dried at 120°C and calcined at 400°C for 16 hours, to decompose and transform the cobalt nitrate to cobalt oxide. The analysis was carried out on 10wt% Co_3O_4/TiO_2 (hereafter referred to as 'Co/TiO_2 catalyst' for convenience), prepared with surface area of $38.75m^2\ g^{-1}$ pore volume of $0.35\ m^3g^{-1}$-1.

3.2.3 Calibrant

The TPR apparatus was calibrated by means of a standard silver oxide (AgO) sample supplied by Sud- chemie. Silver oxide calibration is presented in Appendix 5.

3.3 TPR SYSTEM CONFIGURATION

The instrumentation for TPR investigation is relatively simple. The set-up is as shown in Figure 3.1, with a catalyst sample placed in a reactor in a programmable furnace. The reactor is a quartz tube of 4 mm internal diameter. A thermocouple is used to record the actual temperature of the catalyst bed. The pretreated sample is exposed to a flow of reactive gas mixture, while the temperature is raised (typically at a rate of 0.1-20^{o}C/min) according to a predetermined programme set by a proportional-integral-derivative (PID) controller. (Refer to Appendix 2 for PID controller optimization). Gas valves from cylinders allow the selection of gases to be fed to the reactor. Gas consumption by the catalyst is derived from the change in thermal conductivity of the gas mixture, and detected by a thermo-conductivity detector (TCD). A low gas mixture (5-10% H_2 in Ar) is used to optimize the thermo-conductivity differences between reactant and carrier gas. The hydrogen consumption is monitored and recorded simultaneously with the sample temperature on the computer.

Kinetic analysis of catalysts using TPR technique requires optimal working equipment. This was achieved by making a few modifications to the TPR set-up. Initially the thermocouple was placed in the furnace jacket close to the

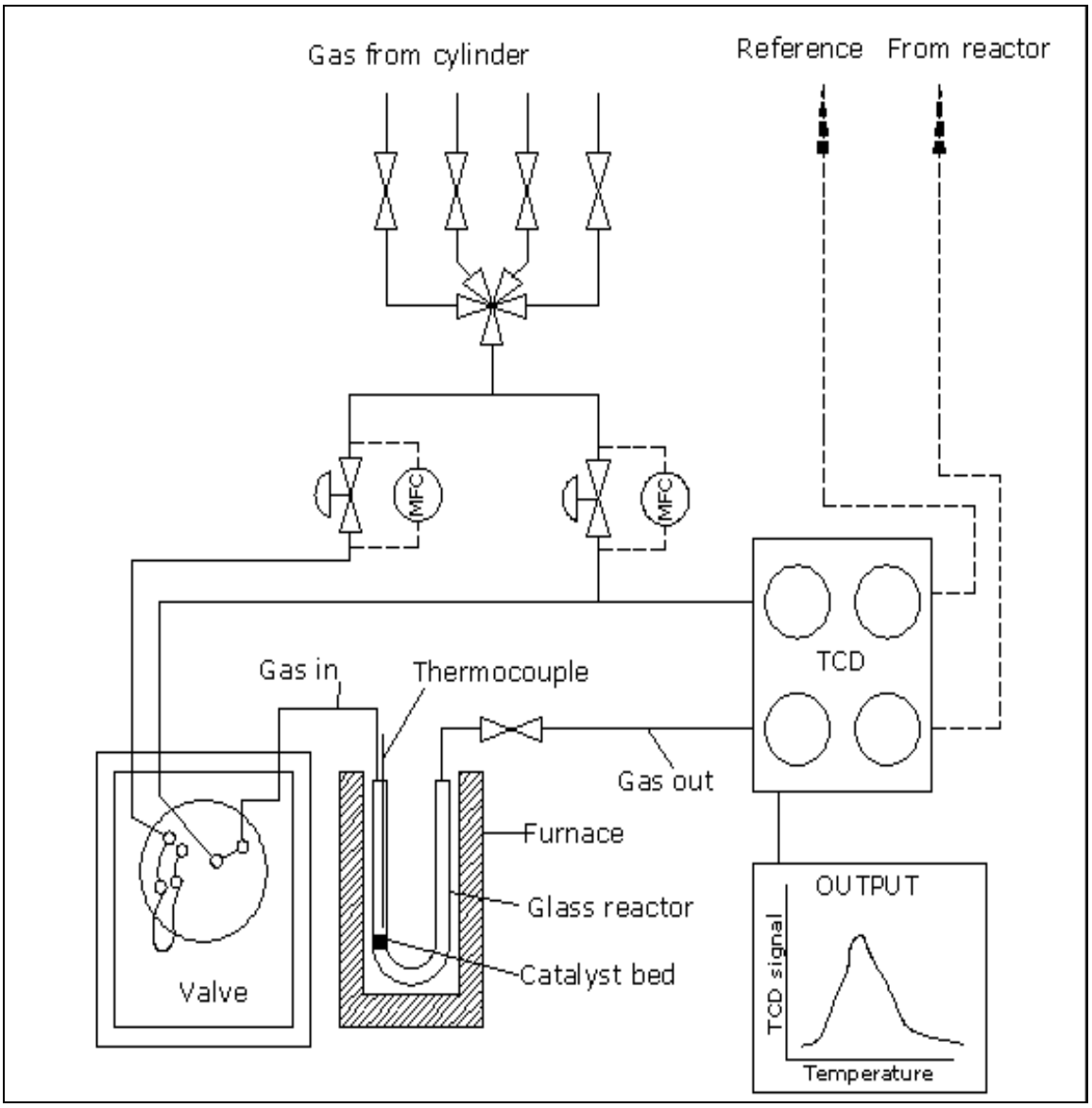

Figure 3.1 TPR Set-up

glass reactor, but later the apparatus was modified so that the thermometer could be positioned inside the reactor, just above the catalyst bed. In this way the actual temperature in that part of the reactor was recorded, and heat

transfer limitations that could cause temperature differences arising from the thickness of the quartz tube were reduced.

The gas flows were initially stabilized by valves and monitored at the exit by flow meters (indicated by dotted lines in Figure 3.1). It was noticed that the flow rate was not stable, and that this affected the reproducibility of the TPR results. The valves were replaced by mass flow controllers (MFC). (Further precautionary measures taken to obtain reproducible TPR profiles are detailed in Appendix 4.)

3.4 EXPERIMENTAL CONDITIONS

It is essential that TPR experiments are carried out under proper laboratory conditions so as to obtain good TPR profiles.

The experiments was carried out under differential conditions to prevent the creation of large H_2 concentration gradients across the catalyst bed. However, it is important to be able to detect the difference in H_2 concentrations between the reactor inlet and outlet with sufficient accuracy. Ways of obtaining approximate experimental factors for optimum sensitivity

were proposed (Monti and Baiker, 1983; Malet and Caballero, 1988). The experimental parameters were optimized in this case to meet the proposed requirements.

3.4.1 Optimization of experimental conditions

The parameters that determine the position of the maximum rate and shape of H_2 consumption peaks are the heating rate β (Ks^{-1}), the initial amount of reducible species n_o (μmol), the flow rate F (cm^3 (NTP) s^{-1}) of the reducing gas mixture and the concentration Co_{H_2} (μmolcm^{-3}) of H_2 in the carrier gas. Monti and Baiker (1983) defined a characteristic number, K, which relates these parameters and facilitates the selection of appropriate values.

For experimentally relevant heating rates between 0.1and 0.3Ks^{-1} this characteristic number is given by equation 3.1:

$$K = \frac{n_o}{F * Co_{H_2}} \quad \text{.....3.1.}$$

K must have values between 55s and 140s for heating rates $0.1 \leq \beta \leq 0.3 Ks^{-1}$, so as to obtain optimum profiles. For values of K below 55s the sensitivity becomes too low, and for values greater than 140s the amount of H_2

consumed is too large. To include the heating rate β, Malet and Caballero (1988) proposed a characteristic number, P, given by:

$$P = \frac{\beta * n_o}{F * \mathrm{Co}_{\mathrm{H}_2}} \quad \text{.....3.2.}$$

The condition for optimum reduction profile is P ≤ 20K.

The experimental parameters have a significant influence on the shape of the TPR profiles, and make it difficult to compare experimental results obtained under different conditions.

Figure 3.2 shows the TPR profiles of a Co/TiO_2 catalyst, and illustrates to what extent the shape and position of the peaks depends on flow rate, heating rate and the mass of the sample.

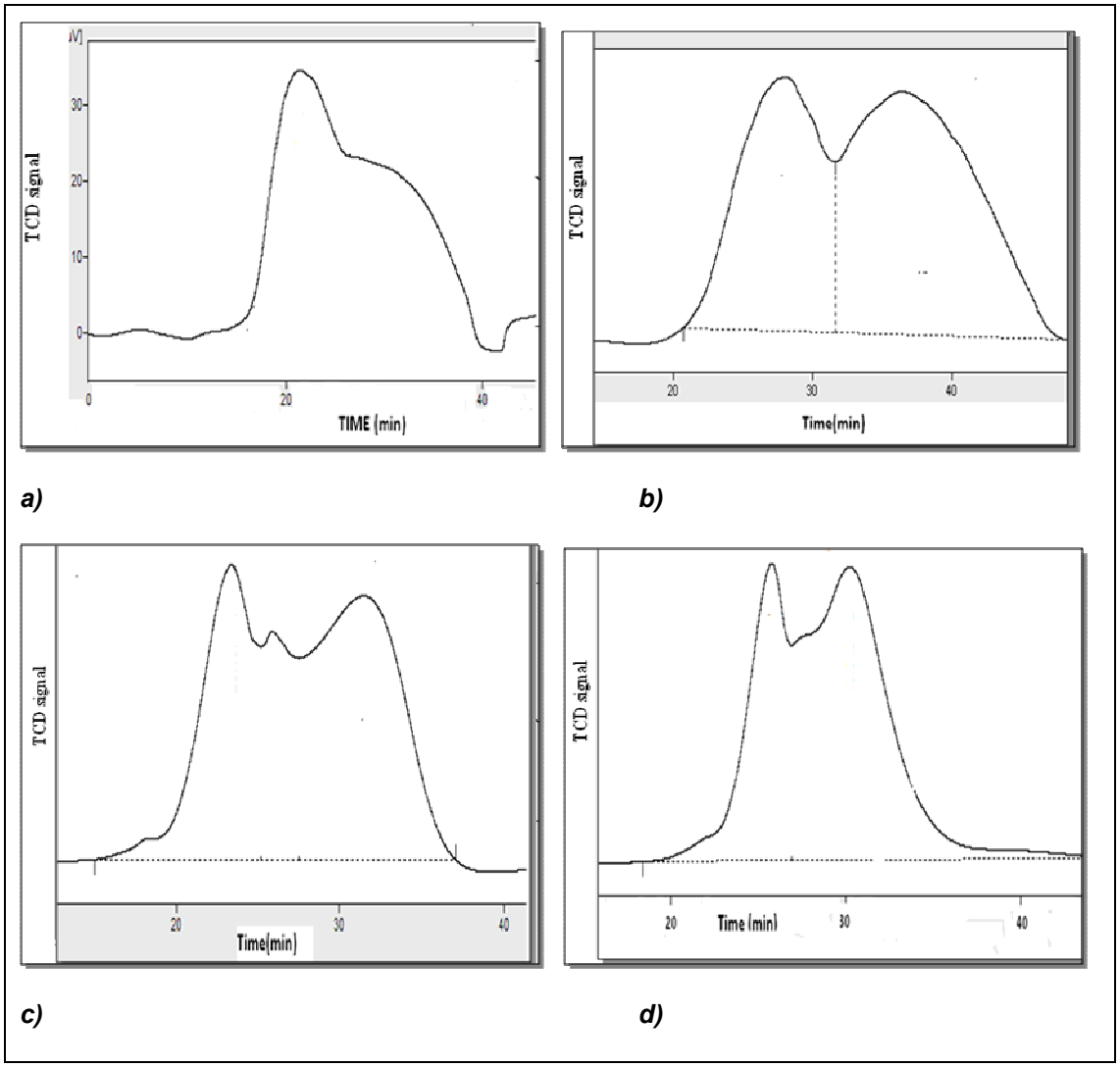

Figure 3.2 TPR conditions (a) catalyst mass-200mg, flow rate-30ml/min, β-10°C/min; (b) catalyst mass-150mg, flow rate 25ml/min, β-10°C/min; (c) catalyst mass-50mg, flow rate 30ml/min, β-10°C/min; (d) catalyst mass-15mg, flow rate 5ml/min, β-10°C/min

The characteristic number P was evaluated for the different parameters used to yield the profiles in Figure 3.2. These are shown in Table 3.1.

Table 3.1 Effect of different parameters on the characteristic number P

profile	*β (K/s)*	n_o *(μmol)*	*F (cc/s)*	Co_{H_2} *(μmol/cc)*	P K
a	0.167	166	0.5	2.2	24.8
b	0.167	124	0.4	2.2	22.4
c	0.167	41.5	0.5	2.2	6.2
d	0.167	12.4	0.08	2.2	11.2

The TPR profile in Figure 3.2 (a) is not distinct, and the value of P is not within the range that gives optimal TPR profiles. The mass of the catalyst and the flow rate was reduced from 200 to 150 g and 30 to 25 ml/min of the reducing gas mixture respectively. Two distinct peaks were obtained, as can be seen in Figure 3.2 (b). However, these peaks were in a 1: 1.5 ratio instead of a 1:3 ratio, as observed in Co catalyst reduction (Yu Lin et al., 2003). This can again be attributed to the value of P, which is beyond the range that gives optimal TPR profiles. In Figure 3.2 (c) the mass of the catalyst was further reduced to 50 mg, whilst the flow rate was kept constant. The value of P was within the suggested range, and a more distinct profile was obtained.

However, a third peak between the two distinct peaks was very pronounced. This was attributed to TiO_2 support, which also reduces under TPR conditions. This assumption was confirmed by TPR analysis of the TiO_2 support, which is shown in Figure 3.3 (a). When the two curves are superimposed, as in Figure 3.3 (b), it can be seen that the TiO_2 support is indeed responsible for the third peak.

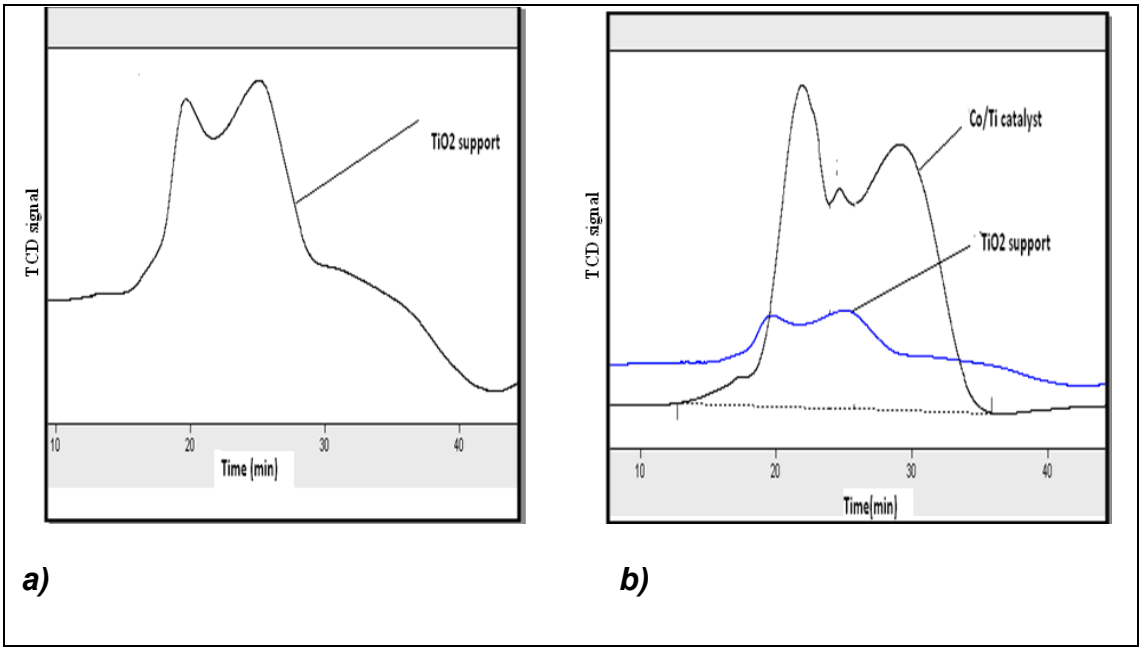

Figure 3.3 *TPR of TiO_2 support (a) Titania support under TPR conditions, titania mass-15mg, flow rate 5ml/min, β=10°C/min (b) merged graphs of titanium TPR profile with Co/TiO_2 catalyst*

It should be noted that the mass of TiO_2 and Co/TiO_2 used in the comparison of the two TPR profiles in Figure 3.3(b) was not the same, because the H_2 uptake caused by the reduction of the support was insignificant when the same mass as Co/TiO_2 was used.

It is interesting to note that although the contribution made by the support in TPR is insignificant, the amount of water produced by the support of catalyst in a 12m long tube may be significant. Therefore, because of the reducibility of the support it would be worth taking its contribution into account when making mass balance calculations involving bulk catalysts.

Since this research described in this chapter was focused on the obtaining kinetics of the Co_3O_4 reduction, the amount of catalyst was further reduced to 15 mg so that the effect on the TPR profile due to the reduction of the TiO_2 support is insignificant. The flow rate was also reduced to 5 ml/min. The parameters were selected to fall within optimal range. As can be seen in Figure 3.2 (d), the peak shapes and temperatures of the maximum reduction rates of the TPR profile attributable to Co_3O_4 reduction are the same as those in Figure 3.2 (c), which confirms that reduction profiles are not influenced by mass transfer effects (Mont and Baiker, 1983). Neither the difference in flow rate nor the amount of catalyst used has influenced the peak shapes and

temperatures of the maximum reduction rates of the Co_3O_4 reduction profile in Figures 3.2 (c) and (d).

The conditions which yield the profile shown in Figure 3.2 (d) were used to select the optimum range for the conditions to be used in this analysis. The initial amount of reducible species n_o and the concentration $\mathrm{Co}_{\mathrm{H}_2}$ were kept constant throughout the analysis, and the choice of the range was based on a varying flow rate. Table 3.2 shows that even when the flow rate is doubled or tripled for the highest and lowest heating rates (10^oC/min and 1^oC/min), the value of P will be within range (that is, ≤ 20K).

Table 3.2 Effect of changes in flow rate on the characteristic number P

β(K/s)	***n_o (μmol)***	***F(cc/s)***	***Co (μmol/cc)***	***P(K)***
0.167	12.4	0.08	2.23	11.2
0.167	12.4	0.17	2.23	5.6
0.167	12.4	0.25	2.23	3.7
0.0167	12.6	0.08	2.23	1.1
0.0167	12.4	0.17	2.23	0.5
0.0167	12.4	0.25	2.23	0.3

Table 3.3 illustrates typical experimental conditions (Lemaitre, J.L., 1984), together with those used in this research.

Table 3.3 Typical experimental conditions for TPR and conditions used in this work

Conditions	**Range/type**
Flow rate (cm3/min)	15–30
This work	5–30
Gas composition	N2+5% v/v H_2
This work	Ar + 5% v/v H_2
Catalyst weight (mg)	100–500
This work	15
Particle size (mm)	0.025–0.25
This work	0.5–1
Heating rate (K/min)	4–60
This work	1–10
Type of detector	TCD
This work	TCD

Kinetic analysis of catalysts using the TPR technique requires optimal working equipment as well as optimal experimental conditions for determining the position of the maximum rate and shape of H_2 consumption peaks.

3.5 TPR PRODUCT ANALYSIS

TPR analysis is based on the reaction of the catalyst sample with a reducing gas (as temperature is progressively increased), where the reaction products at the outlet are detected by the TCD. The configuration of the experimental set-up allows the setting of a required volumetric flow rate into the reactor and from this a quantitative analysis of the products at the reactor exit can be made by mass balance calculations on the TPR system.

3.5.1 TPR mass balance calculations

The material balance for H_2 for a given volume element of a reactor for a given time period is expressed as:

[Moles of H_2 (M_{in}) flowing into the volume element] = [Moles of H_2 (M_{co}) consumed in the volume element] + [Moles H_2 (M_{out}) flowing out of the volume element].

Molar flow rate of H_2 into the reactor can be calculated by:

$F_{in} = \%C_o * Q_m$ 3.3,

where Q_m is the molar flow rate of the gas mixture (mol (NTP) s^{-1}) and $\%C_o$ is percent concentration of reducing gas (for example H_2) in the carrier gas.

Moles of H_2 required for the complete reduction of metal oxide to metal are calculated by means of equation 3.4, where H_2 is used as the reducing gas. Therefore moles of H_2 consumed when the mass of the catalyst and percentage weight of the metal (%wt M) used in the catalyst preparation is known, can be expressed as:

$M_{co} \frac{\%wtM * m_{H_2}}{m_x * mo_{H_2}}$.....3.4,

where %wt is the percentage weight of metal in the catalyst; M the mass of the catalyst sample used in the analysis (g); m_{H_2} and m represent the molar mass of H_2 and metal respectively, based on the stoichiometric equation (g mol^{-1}); and mo_{H_2} is the molar mass of hydrogen (g mol^{-1}).

The total amount of H_2 consumed in complete reduction can be calculated using the total time taken to reduce the catalyst completely, which also allows the calculation of the total amount of water produced. To check H_2 and avoid instantaneous depletion, mass balance calculations are made based on different heating rates. (Refer to Appendix 2 for detailed H_2 mass balance calculations.)

It is important to note that measuring the extent of reduction based on H_2 consumed is possible only if a calibration of the apparatus has been done with a calibrant with a known stoichiometry of reaction with the reducing gas. The rate of reduction can be calculated on the H_2 balance on the system.

The rate of H_2 conversion can be calculated as follows:

$$-rH_2 = \frac{F_{H_2,in} - F_{H_2,out}}{M_{(cat)}} \quad \text{.....3.5,}$$

where: $F_{H_2,in}$ = molar flow rate [moles/min] of H_2 in the reactor feed;

$F_{H_2,out}$ = molar flow rate [moles/min] of H_2 in the reactor outlet gas;

$M_{(cat)}$ = mass of active metal [gramme] of catalyst;

$-rH_2$ = rate of H_2 conversion [moles.min^{-1}.gcat^{-1}].

TPR mass balance calculations can be used to determine the overall rate of reduction, but if a more informative analysis of how rate changes with temperature at different heating rates is required, kinetic analysis can be done on the catalyst. This process is described in Chapter 5.

Mass balance calculations based on the TPR system can be used in fundamental calculations of $\mathrm{P_{H_2O}}$ and $\mathrm{P_{H_2}}$ in a 12 m long tube. However, differences in the conditions (such as operating temperatures and pressure, $\mathrm{P_{H_2O}}$, $\mathrm{P_{H_2}}$ and reducibility of the support used in a 12 m long tube) may have to be considered in comparative calculations.

3.6 IMPLICATIONS AND APPLICATION FOR A 12 M LONG TUBE

When using TPR mass balance calculations for comparative calculations or for developing a model to predict and control P_{H_2O} in a 12 m long tube, certain adjustments have to be made to accommodate the differences in conditions of the two systems. These are summarized in Table 3.4.

Table 3.4 Difference in conditions prevailing in a TPR reactor and a 12 m long tube

	TPR reactor	***12 m long tube***
Tube length (m)	0.3	12
Reactor type used	Fixed bed	fixed bed reactor
Temperatures (^oC/min)	0-800	≤ 500
Operating pressures (atm)	1	.≥ 1
Reducing gas composition %	5-10	Depends on composition mixture
PH_2 inlet gas (atm)	0.05	Depends on composition mixture

Although adjustments can be made that permit mass balance calculations to be used in relation to a 12 m long tube, TPR can be modified to run at conditions similar to those in such a tube, which would make for a more realistic approach and better prediction of P_{H_2O}. The determination of P_{H_2O} can be made beforehand by means of a kinetic model. However, that option is beyond the scope of the research described in this document.

3.7. REFERENCES

1. Acres, G. J. J., Bird, A. J., Jenkns, J. W. and King, F. (1981), *Catalysis Special periodic Reports*, 4, Royal Chem. Soc.,
2. Chronis, T. (1999), PhD Thesis, A Fischer Tropsch Study of Co/Ru Catalysts, University of the Witwatersrand.
3. Duvenhage, D. J. (1993), PhD Thesis, The preparation, characterization and evaluation of Titanium supported Fe:Co Bimetallic Catalysts for hydrogenation of CO, University of the Witwatersrand, South Africa.
4. Lin, H. Y. and Chen, Y.W. (2003), *Thermochimica Acta*, 400, 61-67.
5. Lemaitre, J.L. (1984) Temperature-programmed methods, In Characterization of Heterogeneous Catalysts, Ed. Delannay, F., Marcel Dekker, Inc., New York, 29-70.

6. Malet, P. and Caballero, A. (1988), Journal of the Chemical Society, Faraday Transactions, 84, 2369-2375.
7. Monti, D. A. M. and Baiker, A. (1983), *Journal of Catalysis*, 83, 323-335.
8. Ngwenya, B. D. (2003), MSc Thesis, Process Synthesis for Fischer Tropsch Synthesis, University of Witwatersrand, South Africa.

CHAPTER 4

CONDITIONS AFFECTING REDUCTION IN TPR ANALYSIS

4.0 INTRODUCTION

The reduction process alters the physical and chemical properties of the Co/TiO_2 catalyst, which in turn affect the FT synthesis in terms of reaction rate, activity and selectivity.

Knowledge of which factors influence reduction is essential to understanding the behaviour of the catalyst and determining optimum reduction conditions. In general the more reduced and dispersed the catalyst is, the better. It is evident from previous work that it is possible to control catalyst dispersion through either the amount of water removed prior to reduction (Anderson et al., 1970) or the heating rate and partial pressure of water during reduction (Andrew et al., 1976).

According to the published literature (Dzis'Ko et al., 1975; Bartholomew and Farrauto, 1976; Haong-Van et al., 1986; Chen and Shiue, 1988; Kruissink, 1981; Rostrup-Nielsen, 1972; Bertole et al., 2002), the main parameters affecting the extent of reduction are temperature, reduction duration, heating rate, space velocity and the gas composition used in the process.

Starting with the first of these, it has been found that the reduction temperature strongly affects the properties of the catalyst, such as extent of reduction, surface area and dispersion (Dzis'Ko et al., 1975; Bartholomew and Farrauto, 1976; Haong-Van et al., 1986 and Chen and Shiue, 1988). The space velocity of H_2 was also reported as affecting the surface area of the catalyst, in that an increase in space velocity caused a corresponding growth in the active surface area (Kruissink, E. C., 1981). Another finding was that a large catalyst surface area and high dispersion were obtained at a low flow rate. Many researchers (Kruissink, 1981; Bartholomew and Farrauto, 1976; Haong-Van et al., 1986) have observed that the reduction duration time affected catalyst characteristics. In addition, the heating rate during reduction was found to affect the catalyst's properties (Dzis'Ko et al., 1975; Bartholomew and Farrauto, 1976; Haong-Van et al., 1986 and Chen and Shiue, 1988), and the presence of steam in H_2 to decrease the area of the catalyst (Rostrup-Nielsen-Nielsen, J. R., 1972 and Bertole et al., 2002).

This chapter presents a comparative study of catalyst behaviour using TPR operated at two extremes, that is i.e. the lowest and highest parameter values within the TPR- recommended range of conditions. The behaviour of catalysts in TPR at these two extremes enabled a quick evaluation of the effect of different parameters on the extent of Co/TiO_2 catalyst reduction, which in turn facilitated an assessment of what this would imply for the behaviour of the catalyst in a 12 m long tube. This information was also applied in the design of reduction procedures involving bulk catalysts.

4.1 Effect of flow rate on the extent of reduction

To investigate the effect of flow rate on the extent of reduction of a Co/TiO_2 catalyst, a fixed amount of catalyst (15mg) using a ramping temperature of 10^oC/min with two different flow rates, 5ml/min and 30ml/min of 5% H_2/Ar, was used. The reaction was run by ramping the temperature to a range of temperatures (175, 200, 250, 300, 350 and 400^oC). TPR runs were performed in this way to determine how flow rate affects the amount of H_2 consumed as the final temperature is increased.

To gain a more realistic insight into how catalysts in a 12m tube would behave, the final TPR temperatures are kept low (below 500^oC), to replicate those in industrial operations.

The total amount of H_2 consumed was evaluated for each experiment. The results are given in Table 4.1 and Figure 4.1.

Table 4.1 Effect of flow rate and final temperature on the H_2 consumed

Flow rate (ml/min)	*Final temperature (^oC)*	*Hydrogen consumed (µmol)*
5	175	1.2
	200	5.1
	250	14.1
	300	27.5
	350	34.0
	400	41.8
30	175	2.6
	200	5.2
	250	16.9
	300	27.4
	350	36.2
	400	42.1

It can be seen that the flow rate does not have a significant effect on reduction. Figure 4.1 shows that the overall amount of H_2 consumed is not significantly different at a higher flow rate (30ml/min) than at a lower (5ml/min). According to the background literature, H_2 interacts with CoO to produce water which, if not removed from the catalyst's surface, encourages the transport and growth of Co crystallites (Kruissink, E. C., 1981). This however would appear not to be a problem at the conditions in the tests.

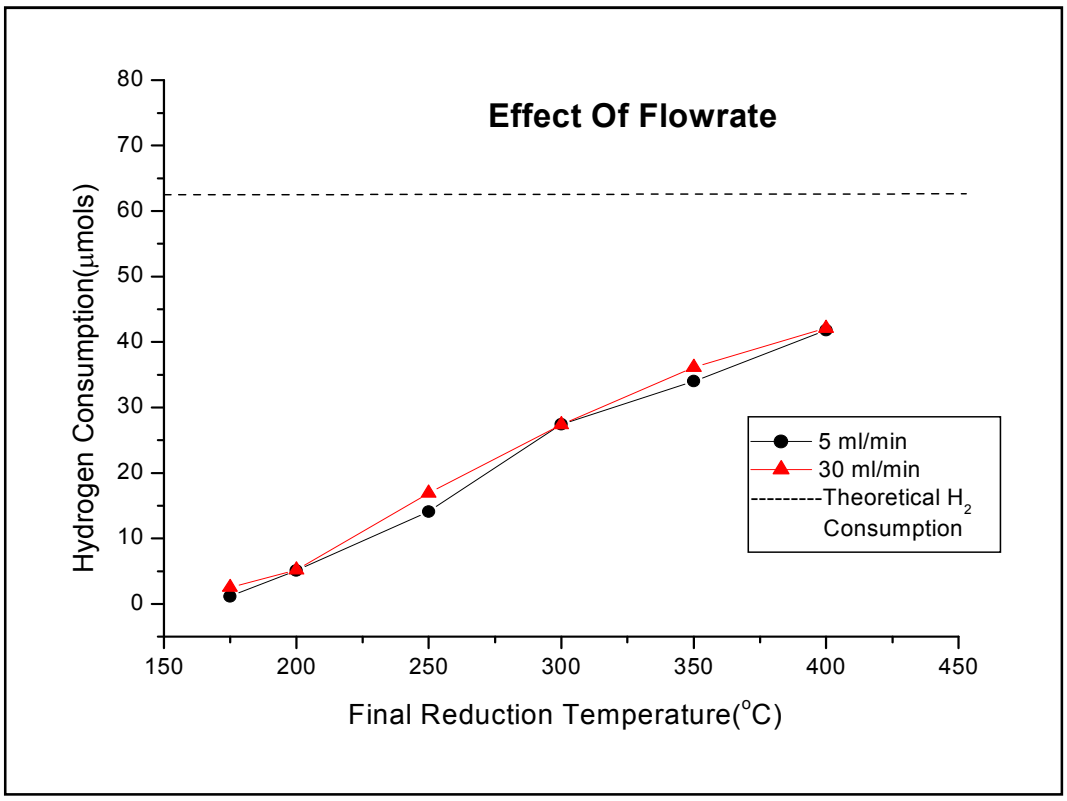

Figure 4.1 *Effect of flow rate on the extent of reduction*

It is worth noting that Figure 4.1 shows that the lines for experimental hydrogen consumed lines do not approach the theoretical limit of H_2 consumption, which indicates that reduction is not complete.

4.2 Effect of ramping temperature on the extent of reduction

To analyze the effect of ramping temperature on reduction, temperature at the rates of 1 and 10^{o}C/min respectively to reach the various final temperatures (250, 300, 350 and 400^{o}C) shown in Figure 4.2. A flow rate of 5ml/min of 5% H_2/Ar and the same mass of 15mg was used in the analysis.

At each of the reduction temperatures, the amount of H_2 consumed was evaluated for that particular TPR profile.

It is evident from the steepness of the peaks in Figures 4.2 (a) and (b) that reduction is much more gradual at the lower ramping rate. At the lower final temperatures the second peak is not formed, which suggests that the second step of reduction occurs mainly at temperatures above 300^{o}C.

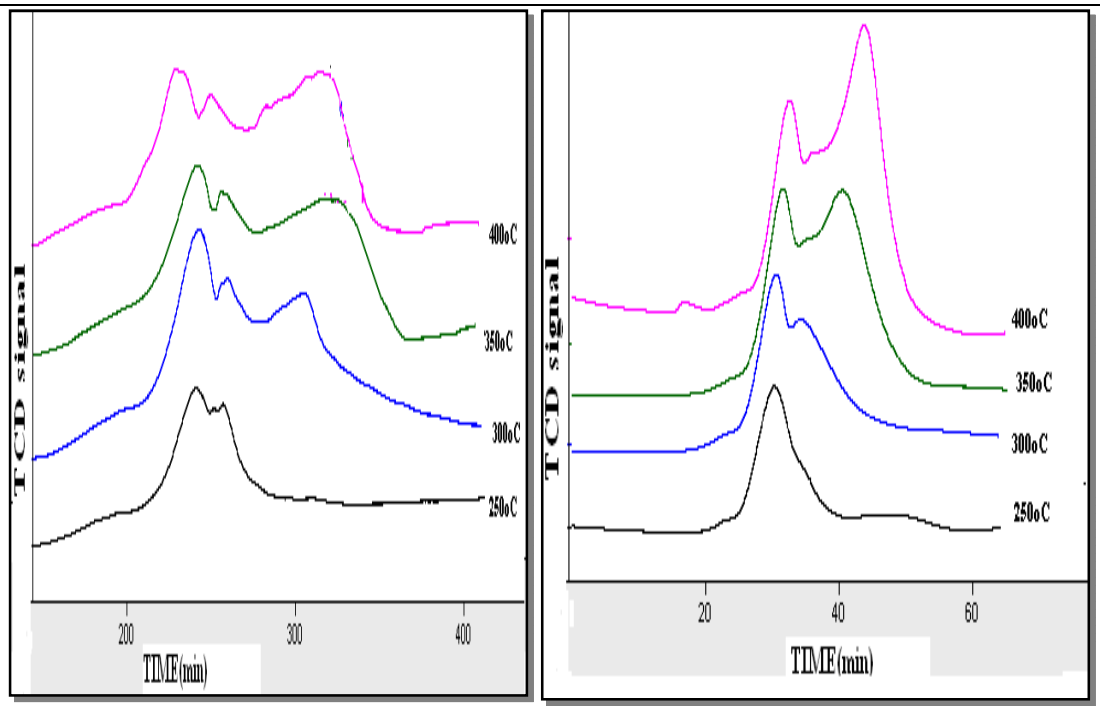

a) 1°C/min b) 10°C/min

Figure 4.2 *Effect of heating rate (a) at 1°C/min (b) at 10°C/min on reduction*

Table 4.2 shows the total amount of H_2 consumed at the two ramping rates for the various final temperatures.

Table 4.2 Effect of ramping rate and final temperature on the amount of H_2 consumed

Ramp temperature (^oC/min)	***Final temperature (^oC)***	***H_2 consumed (μmol)***
1^oC/min	175	2.8
	200	3.7
	250	15.7
	300	40.2
	350	40.8
	400	41.1
10 ^oC /min	175	2.8
	200	3.1
	250	14.1
	300	27.5
	350	34.0
	400	41.8

At the lower heating rate (1^oC/min) the amount of H_2 consumed increases in proportion with the temperature until it reaches a limiting extent of reduction at 300^oC. However, at the higher heating rate (10^oC/min), the amount of H_2 consumed continues to increase linearly with temperature, and reaches a

limiting extent of reduction only at 400°C. Consequently, the extent of reduction achieved is the same in both cases at the highest final temperature of 400° C.

As Figure 4.3 shows, for both ramping rates the amount of hydrogen consumed with temperature in relation to temperature is not very significant at low temperatures (betweeen175–250°C), but the graph slopes are comparatively steeper for both ramping rates above 250°C.

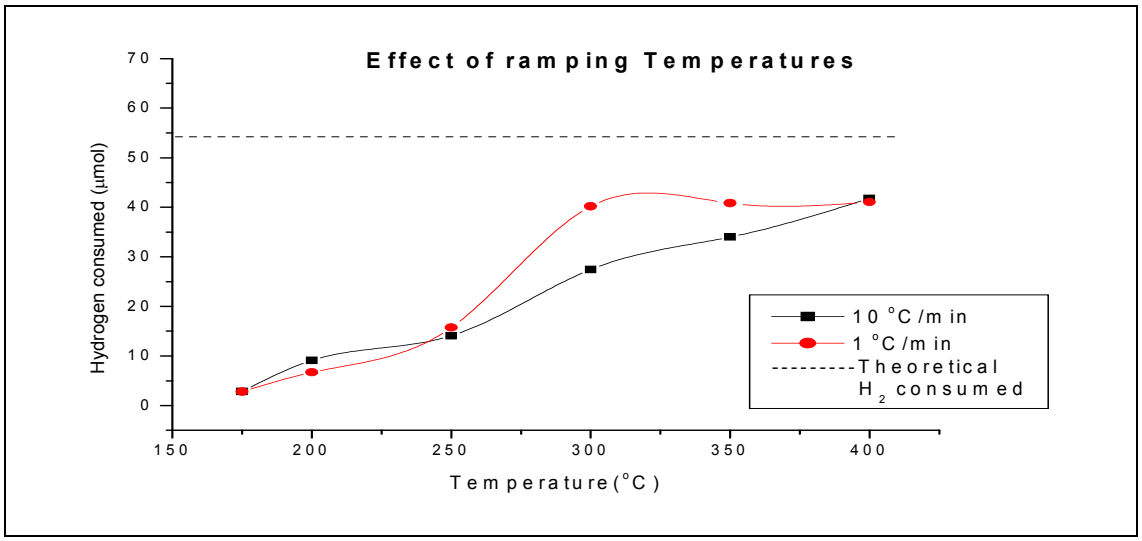

Figure 4.3 *Effect of ramping temperature on amount of H_2 consumed*

This suggests that the rate of reduction is fairly slow at first (when the temperatures are below 250°C), and accelerates as the temperature increases (above 250°C).

The trends in Figure 4.3 for both ramping rates resemble those observed in the nucleation and growth model discussed in Chapter 2. According to that theory, the dissociation of H_2 is very slow initially. However, once the nucleus of the reduced metal is available, it acts as a catalyst for further reduction by providing a site on which hydrogen is disassociated. A low heating rate allows more sites to be created for H_2 dissociation. After this stage, reduction is very rapid and depends on the available dissociated hydrogen radicals.

Bartholomew and Farrauto (1976) achieved a similar result using thermal gravimetric analysis to study the effect of ramping rate on a Ni/Al_20_3 catalyst in a hydrogen atmosphere. They suggest that hydrogen interacts with the catalyst oxide to produce water which, if not removed from the catalyst surface, encourages the transport and growth of metal crystallites. A further observation made was that a slow heating rate allowed water to be driven off and transported from the catalyst's surface by the flowing stream of hydrogen, in this way minimizing the effect of sintering.

4.3 Effect of a catalyst particle diameter cut

Two particle cuts were used to investigate the effect of catalyst grain size on the quantity of hydrogen consumed in a Co/TiO_2 catalyst. One sample was crushed (<425μm), while the other was in the size range 800-425 μm. The

ramping temperature set at 10^{o}C /min and a flow rate of 5ml/min of 5% H_2/Ar was used on a catalyst mass of 15 mg throughout.

Table 4.3 Effect of a catalyst particle diameter cut on the quantity of H_2 consumed

Catalyst size (μm)	***Temperature (^{o}C)***	***H_2 consumed (μmol)***
800-425	175	2.8
	200	9.1
	250	14.1
	300	27.5
	350	34.0
	400	41.8
<425	175	2.6
	200	3.9
	250	14.1
	300	20.7
	350	30.8
	400	31.9

The reaction was run by ramping the temperature to various final temperatures, as in the previous analysis. Hydrogen consumption was evaluated at each reduction temperature for the different particle cuts, as shown in Table 4.3 and Figure 4.4.

The amount of hydrogen consumed initially, for a final temperature between 175–about 250 ^{o}C, was almost the same, as is shown in Table 4.5 and Figure 4.4. However, at higher temperatures the amount of H_2 consumed and thus the extent of reduction on the uncrushed sample proved higher than on the

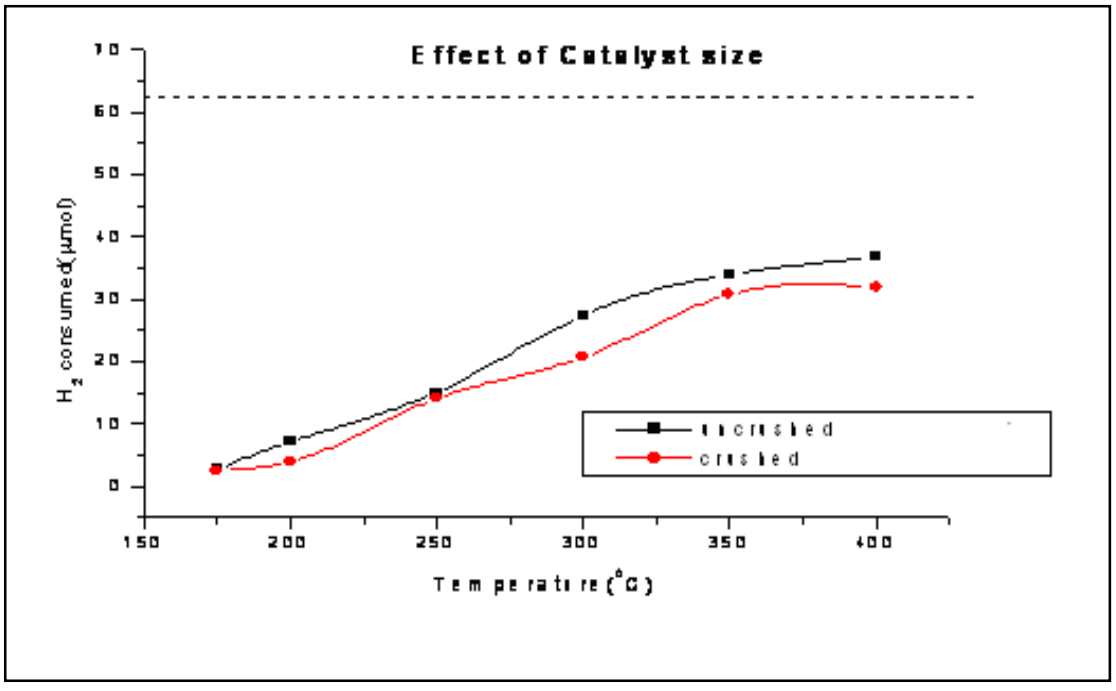

Figure 4.4 *Effect of catalyst particle diameter cut and final reduction temperature on the amount of H_2 consumed*

crushed sample. Although the difference is not very significant, this observation is rather contradictory. The higher degree of reduction would be expected on the crushed catalyst rather than on the uncrushed catalyst because of the larger catalyst surface area available on the former.

One possible explanation for this finding is that the water content of the catalyst prior to reduction has an effect on the total hydrogen consumed. Water could have been readsorbed on the catalyst during exposure to laboratory air prior to reduction, while the rate at which water was removed depended, first, on the drying period prior to reduction, where catalysts are dried in the argon flow system as the temperature is raised. Second, the rate at which water was removed is contingent on the size of the catalysts. At a constant argon flow rate, the small catalysts are drier at the time of reduction than the bigger ones.

To gain more insight, the effect on the total amount of hydrogen on the drying time prior to reduction was investigated. This is presented in the next section.

4.4 Effect of drying time prior to reduction on the extent of reduction

A sample of uncrushed (800–425 μm) and one of crushed (< 425 μm) catalyst were subjected to the same drying time prior to reduction by TPR to examine

the effect of drying time on the total amount of hydrogen consumed. Argon gas of 99% purity was used as the drying agent. Both samples were ramped at 10^{o}C/min to 150^{o}C and at a flow rate of 5ml/min, and each had the same mass of catalyst (15 mg). TPR runs were carried out after the respective samples had cooled to room temperature, under the flow of argon. A ramping temperature of 10^{o}C/min, from room temperature to 800^{o}C, was used. Figure 4.5 shows the TPR profiles of crushed and uncrushed samples subjected to the same drying period (50 minutes at 150^{o}C) prior to reduction by TPR.

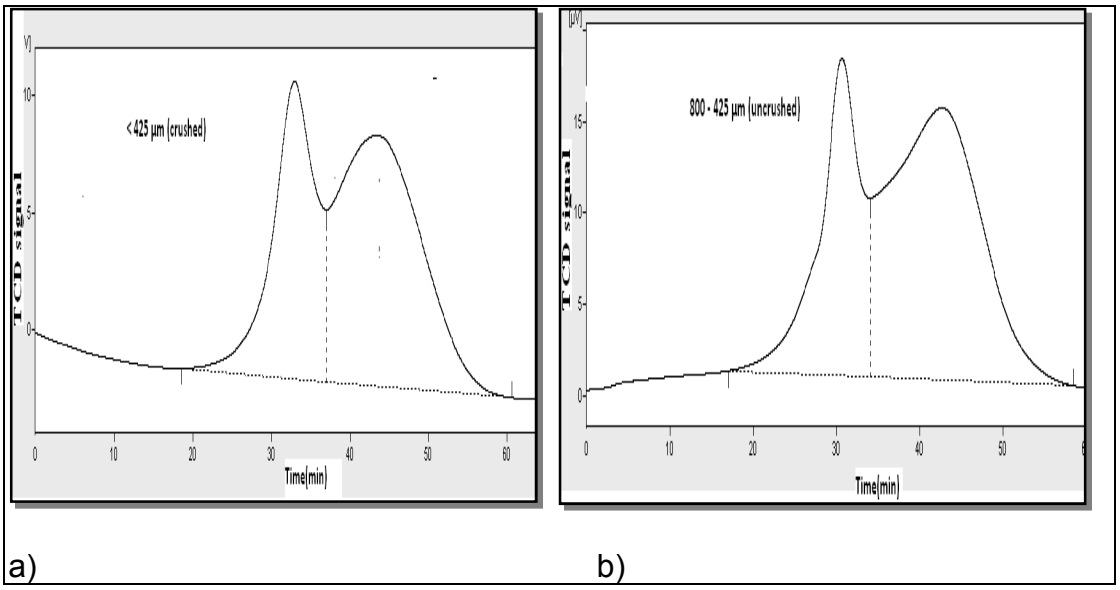

Figure 4.5 *Drying time of 50 minutes. The amount of H_2 consumed by (a) uncrushed catalyst (b) crushed catalyst*

It can be seen from Table 4.4 that the amount of H_2 consumed in the uncrushed catalyst is higher by about 24% than in the crushed catalyst.

Table 4.4 Effect of drying times on uncrushed and crushed catalyst samples

Catalyst size (μm)	***Total drying time (min)***	***H_2 consumed (μmol)***
<425(crushed)	50	32.0
800-425(uncrushed)	50	41.8

Figure 4.5 shows that there is no change in peak position, which implies that there are no heat transfer limitations related to particle size.

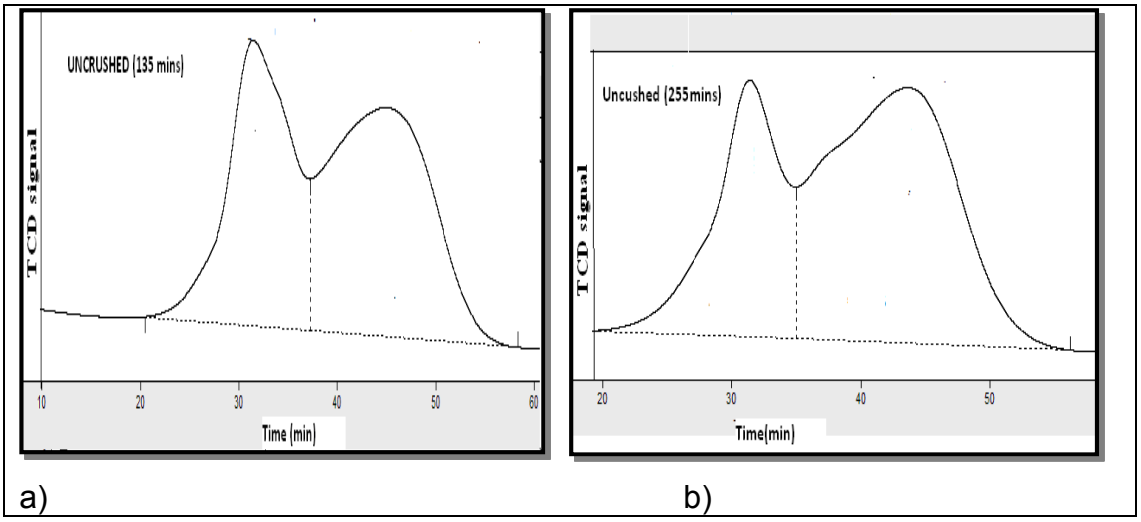

a) b)

Figure 4.6 *Effect of drying time on the uncrushed catalyst (a) Uncrushed cobalt catalyst dried for 2hrs 15min (b) Uncrushed cobalt catalyst dried for 4hrs 15mins*

Two other samples of uncrushed catalyst of the same mass were dried for 155 and 255 minutes respectively at 150^{o}C using a ramping rate of 10^{o}C/min. The same TPR procedure used previously was employed. The TPR profiles of uncrushed catalysts with different drying times are shown in Figure 4.6.

A summary of the results obtained is given in Table 4.4

Table 4.5 Effect of drying times on H_2 consumed

catalyst size (mm)	***Drying time at 150^{o}C (min)***	***H2 consumed (µmols)***
800-425	50	41.8
	135	33.7
	255	31.4

It can be seen from Table 4.4 that the total amount of hydrogen consumed reduces significantly with an increase in the drying time prior to reduction by TPR. A similar observation was made by Anderson et al. (1970), who used electron microscopy and hydrogen chemisorption on 5% Pt-Cu catalysts to study the effect on crystallite size of drying time prior to reduction. They reported that those catalysts that had been exposed extensively to laboratory

air between drying and reduction had larger crystallites than those that were reduced immediately after drying. They also noted that catalysts that were reduced in smaller batches had smaller crystallites than those reduced in bigger batches.

However, a conclusive explanation of why more hydrogen was consumed in the catalyst which that had a shorter drying time was not offered. Poisoning caused by impurities in the gas stream could not have been the reason because the results were consistent, even when different samples were used and the gases used were certified as ultra-high quality. Possible answers include the following:

(i) The drying time could have caused the catalysts to agglomerate or sinter, which would make it difficult to reduce the outer surface.

(ii) Water affects the TCD reading, and results in higher readings commensurate with the water content of the catalyst. It could be postulated that the catalyst dried for a shorter period had a higher water content overall because the reading from the TCD gives not only the amount of the water driven off by heating in the TPR procedure but also the water produced by reduction of the catalyst.

For greater insight on this subject, FT runs could be performed on samples with different levels of water content to investigate and quantify the effect that drying the catalyst prior to reduction would have on its activity.

4.5 APPLICATION AND IMPLICATIONS FOR A 12M LONG TUBE

The results presented in this study show how different reduction conditions affect the extent of reduction of the Co/TiO_2 catalyst.

The trend shows that in a laboratory-scale reactor, flow rate has little or no effect on the extent of reduction. However, for a 12 m long tube it may be more desirable to use a higher flow rate which will aid the removal of water from the catalyst's surface and in turn will help to reduce the transport and growth of Co crystallites.

Given a choice of reducing conditions for a Co/TiO_2 catalyst, it is advantageous to reduce at a lower ramping rate, so as to maximize the extent of reduction to active Co metal in bulk catalyst. Moreover, a limiting extent of reduction point is reached at lower temperatures when a lower ramping rate is used than when the ramping rate is higher. The lower reduction temperatures also prevent overheating.

The grain size of the catalyst does not affect the extent of reduction, although the water content does. It is important to note that none of the conditions used in this study was the extent of reduction more than 70% relative to that when complete reduction (100%) is assumed. The effect of this on the catalyst performance and activity needs to be studied further.

This chapter demonstrates through practical testing the extent to which catalyst reduction depends on certain conditions, and illustrates the need for careful consideration of which reduction conditions are required for stable and optimally effective catalysts. To evaluate how different parameters affect the activity of the catalyst in a 12 m long tube, It would be helpful to perform FT experiments using different pretreatment and reduction procedures. By these means optimal reduction conditions can be designed based on both the extent of reduction and on catalyst activity.

4.6 REFERENCES

1. Anderson, J. H., Conn, P. J. and Brandenburg, S. G. (1970), *Journal of Catalysis*, 56, 356.
2. Andrew, S. P., Delmon, B., Jacobs, P. A, and Poncelet, G. (1976), Eds, *Elsevie*r, Amsterdam, 429-444.

3. Bartholomew, C. H. and Farrauto, R. J. (1976), *Journal of Catalysis*, 45, 41.
4. Bertole, C. J., and Mimms, C. A. (2002), *Journal of Catalysis*, 210, 84-96.
5. Chen, I. and Shiue, D. W. (1988), *Industrial Engineering Chemical Research*, 27, 429.
6. Dzis'ko, V. A., Nsokova, S. P. and Borisova, M. S. (1975), *Kinetic Catalysis*, 15, 667.
7. Hoang-Van, C., Villeman, B. and Teichner, S. J. (1986), Reactor, *Kinetic Catalysis Letters*, 26, 127.
8. Kruissink, E. C. (1981), PhD Thesis, Delft University Press, Delft, Netherlands.
9. Niemantsverdriet J. W., *Spectroscopy in Catalysis: An Introduction*, Edittion 3, 2007, Eindhoven University of Technology, the Netherlands.
10. Poltorak, O. M and Bozonin, V. S. (1965), *Journal of Physical Chemistry*, 39, 781.
11. Rostrup-Nielsen –Nielsen, J. R. (1972), *Journal of Catalysis*, 27, 343.

CHAPTER 5

KINETIC MODELLING OF TPR ANALYSIS

5.1 INTRODUCTION

TPR profiles contain a great deal of information that can be used to obtain the kinetics of catalyst reduction, even in complex cases, which can be used to describe both the mechanism of reduction and the temperature-sensitivity of the rate of reduction. These functions are achieved by means of the kinetic triplet; activation energy (E_a), reaction model (f (α)), and pre-exponential factor (A). Because the evaluation of kinetic parameters in TPR reduction should be independent of the reactor used, the information can be applied to kinetic analysis of the basic reduction of catalysts in a 12 m long tube.

This chapter presents a kinetic evaluation of a Co/TiO_2 catalyst that is not based on obtaining accurate kinetic data, but instead focuses on understanding the mechanism of reduction and the manner in which temperature affects the rate of reduction at different heating rates. This information is then applied to the study of the behaviour in a 12 m long tube.

Kinetic modelling of Co/TiO_2 two-step reduction was carried out by separating the two peaks and analyzing them individually. By this means, the effect of temperature on the rate of reduction at each heating rate could be evaluated at every stage of reduction. This approach was found to be helpful because the data were more easily quantified, and therefore provided a good basis for an understanding of the complex reduction kinetics of this catalyst.

The Friedman method was used to obtain estimates of activation energies at each point in the reduction. In addition Málek's method was applied to simulate the experimental data for both the first and second peaks.

5.2 EXPERIMENTAL PROCEDURE

5.2.1 TPR measurements

TPR experiments were carried out using 5% H_2/Ar (flow rate, 5ml/min; pressure, 1bar) as the reducing gas and a sample mass of 15 mg. All of the experimental conditions were in agreement with those recommended by Monti and Baiker (1983). Prior to each TPR run the catalyst was degassed and dried under pure Argon gas at a rate of 10^{o}C/min to 150^{o}C, and then left for 20 minutes at 150^{o}C. This improved the baseline of the TPR profile. TPR

runs were carried out after the sample had cooled to room temperature under the flow of argon, and the consumption of H_2 measured with a TCD. A variety of ramp temperatures of 3, 5, and 10^{o}C/min, from room temperature to 800^{o}C, were used in all of the experiments.

5.3 RESULTS AND DISCUSSION

The H_2 TPR thermograms (β=3, 5 and 10^{o}min), measured for the Co/TiO_2 catalyst, are shown in Figure 5.1. The experimental data clearly exhibit a two-step reduction. The first peak is assumed to be due to reduction of Co_3O_4 to CoO:

$Co_3O_4+H_2 \rightarrow 3CoO+H_2O$…..……...5.1,

while the second is assumed to be due to the reduction of CoO to metallic cobalt.

$CoO + H_2 \rightarrow Co + H_20$ ……..5.2.

These results are consistent with those recorded in previous studies (Wan et al, 2007 and Lin and Chen, 2007).

The maxima for the two peaks at each heating rate are given in Table 5.1,

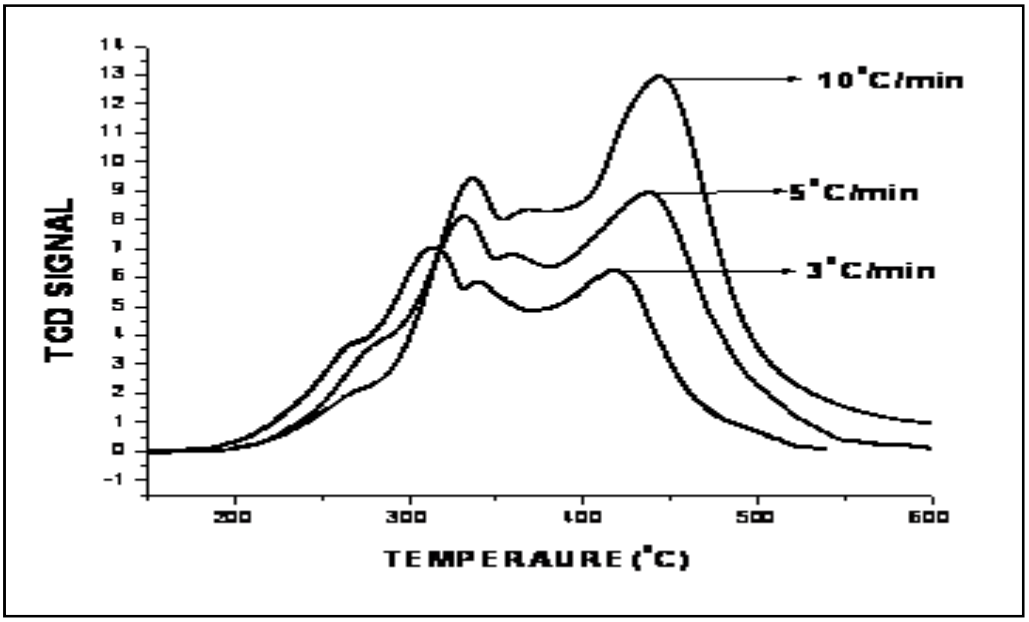

Figure 5.1 *TPR profiles for the reduction of Co/TiO_2 catalyst at heating rates: 3, 5 and 10^oC/min.*

which shows the effect of the ramping rate on temperatures for the complete reduction process of a Co/TiO_2 catalyst using hydrogen gas. T_o is the initial temperature, Tp_1 the first peak temperature, Tp_2 the second peak temperature, T_f the final temperature and ΔT the temperature difference between T_f and T_o.

Table 5.1 Effect of heating rate on the characteristic temperatures of reduction process

β ($^{o}C/min$)	T_o (K)	Tp_1 (K)	Tp_2 (K)	T_f (K)	ΔT (K)
3	473	583	693	783	310
5	498	606	715	798	308
10	493	625	753	883	390

The measurements in Table 5.1 show that at a lower ramping rate reduction starts at a lower temperature than is the case when a higher ramping rate is employed.

5.3.1 TPR profile evaluation

The Co catalyst undergoes two separate reactions ($Co_3O_4 \rightarrow CoO \rightarrow Co$) before the catalyst is completely reduced, which is why the peaks are evaluated independently. However, the two reduction peaks overlap, making separation a challenge. To solve the problem, it could be postulated that the peaks are fairly symmetrical, and that therefore, if the first reaction was allowed to reach completion before proceeding to the second one, two separate, symmetrical

and complete curves would be obtained. A Gaussian curve could then be fitted to the two profiles and the two steps of reduction analyzed individually. Although the Gaussian curve does not fit the respective profiles exactly, it simplifies the analysis of data by providing an equation that can be used to complete the profiles for the two separate reduction steps.

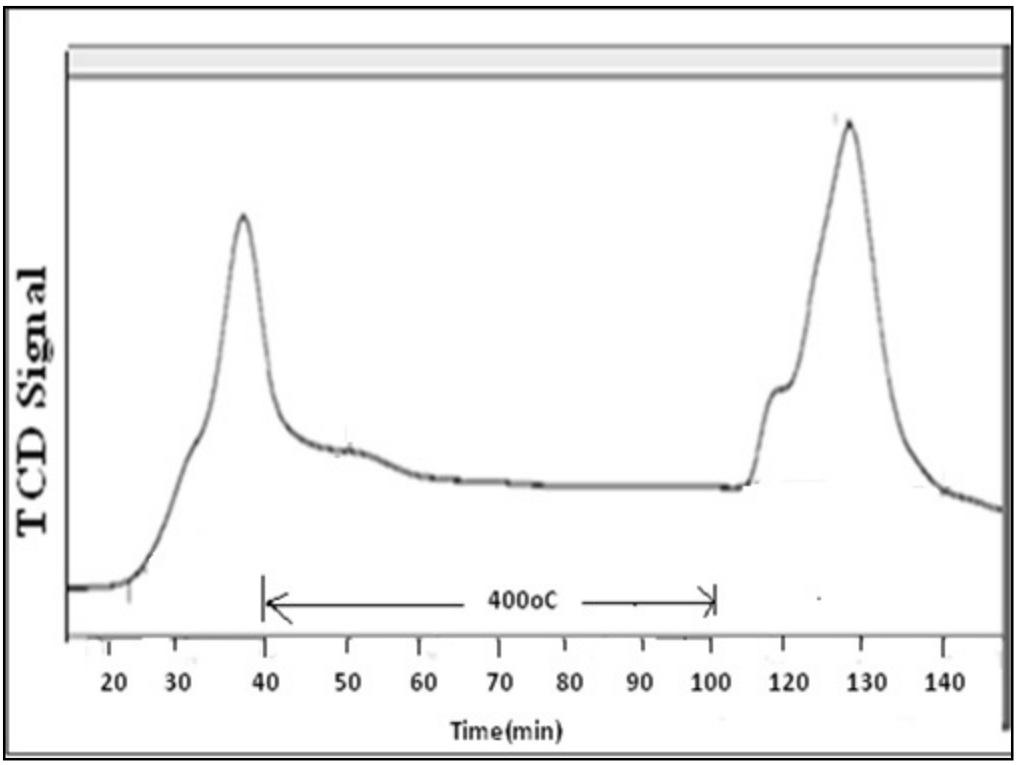

Figure 5.2 *Separated Co/TiO_2 peak*

To show that the two peaks are separable and fairly symmetrical when using TPR, the temperature is ramped to a constant temperature (350^{o}C), at which the first reaction is completed, and the temperature kept constant for one

hour to allow for a good baseline. After that the temperature was ramped up again to complete the second peak. This process is shown in Figure 5. 2. Temperatures were ramped to various temperatures to obtain two separate relatively distinct peaks and this is illustrated in appendix 6.

The two small peaks observed, one below 300^{o}C before the first peak and the other around 400^{o}C, are attributable to reduction of the TiO_2 support, as shown in Chapter 3. (The contribution of the TiO_2 support was not included in the kinetic analysis.)

The Gaussian Probability Function (Gpf) can be fitted to the TPR profiles shown in Figure 5.1, and the resultant data used for further kinetic analysis of the two steps of Co/TiO_2 reduction.

The following relationship, based on Gpf, can be written as follows:

$$(\frac{d\alpha}{dT})_{T,\beta} = (\frac{d\alpha}{dT})_{onset} + \frac{A}{\sqrt{\frac{\pi}{2}}} exp\, -2(\frac{T_{ac}-T_m}{w^2}) \quad \text{.....5.3,}$$

where

$(d\alpha/dT)_{T,\beta}$ = the change of α with temperature at a consider heating rate;

$(d\alpha/dT)_{onset}$ = dα/dT at the onset temperature;

T_{ac} = actual temperature at a considered heating rate;

T_m = temperature at the centre of the peak (dα/dt = 0);

A = area under the curve; and

w = width parameter

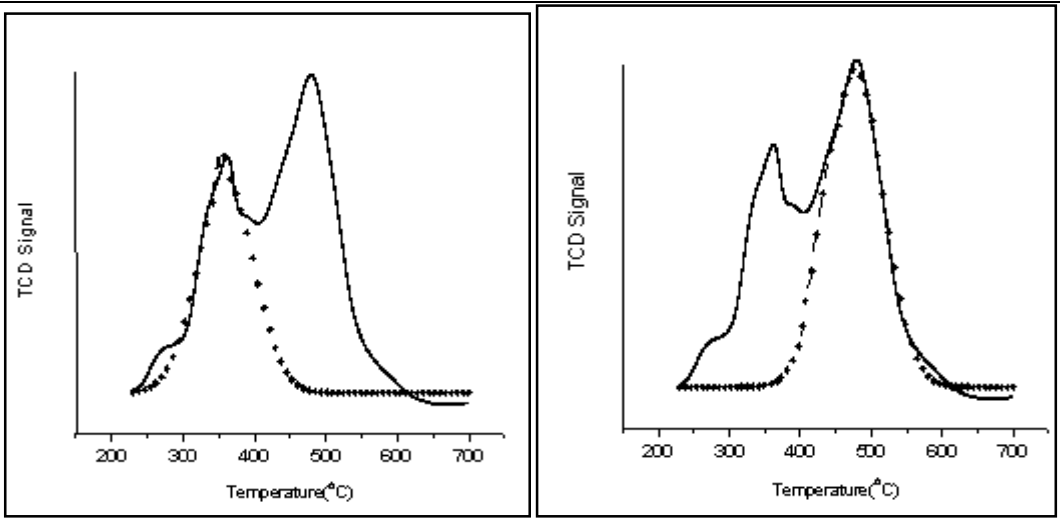

a) Gaussian model fitted in the first peak (b) Gaussian model fitted in the second peak

Figure 5.3 *Gaussian model fitted in the first and second peaks*

The Gpf was fitted into the individual peaks of the complete Co/TiO_2 reduction profile, as shown in Figure 5.3 (a,b).The Gaussian curves fit the cobalt profile well and can thus be used for further kinetic analysis. If the two reduction

peaks are separated, the complete TPR profile maintained and the reduction profile due to TiO_2 ignored, the postulated TPR profile would resemble that given in Figure 5.4.

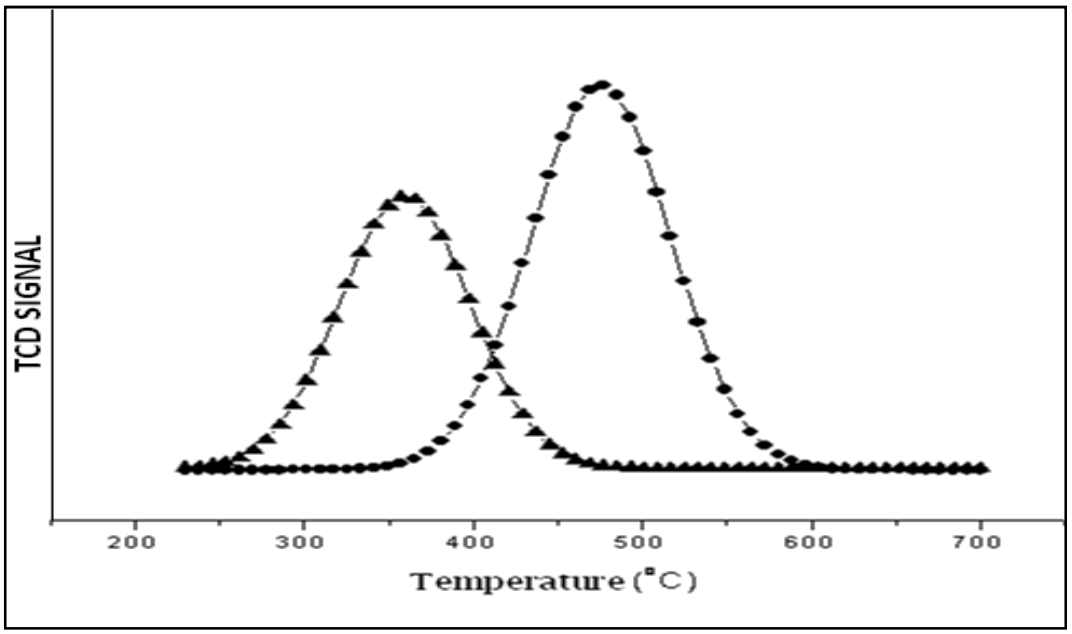

Figure 5.4 *Gaussian curves for first and second peak of cobalt catalyst reduction*

Table 5.2 gives numerically evaluated fitting parameters based on the heating rates using Gpf. The width parameter that determines the shape of the curve remains constant at different heating rates for the first and second peaks respectively. This shows that Gpf provides a good fit for experimental data, since the shape does not change in the experimental TPR profiles for the different peaks.

Table 5.2 The influence of heating rate on the numerically fitting parameters (w, A) (Equation 4.1) for the reduction of Co/TiO_2 catalyst

B ***(°C/min)***	***w***	***h***	***T_p*** (°C)	***A[a]***	***R^2***	***Chi-square***	***Extent of reduction (based on total H_2 consumed)[b]***
1st peak							
3	78.9	7.2	333.8	24152	0.998	0.026	27.3
5	78.5	7.7	333.8	24662	0.998	0.0525	27.9
10	78.3	11.4	359.81	24712	0.997	0.060	28
2nd peak							
3	68.3	6.3	411.5	44456	0.986	0.0806	50.3
5	68.1	8.2	432	45221	0.989	0.1064	50.6
10	68.4	16.4	475	44896	0.986	0.53	50. 5
Total 1st + 2nd profile (Gpf)				69366	(Average for all heating rates)		78.5
Total experimental TPR profile				*74669*	Average for all heating rates)		84.5

[a] *A is the area under the profiles multiplied by the flow rate (5ml/min)*

[b] *The extent of reduction is based on the total hydrogen consumed for complete reduction of $Co_3O_4TiO_2$ evaluated using AgO as the calibrant as shown in appendix 5.*

The fitted Gaussian curves were then analyzed individually

The data obtained from the Gaussian fits was then used to evaluate the extent of reduction at the individual peaks. Based on equations 5.1 and 5.2 the expected ratio of integrated areas of the first peak to second peak is 1:3. However this is not the case for the areas in Table 5.2 where the ratio is 1:2. This is attributed incomplete reduction of Co/TiO_2. Theoretically 25% of the of the total Co/TiO_2 reduced would be a result of reduction from Co_3O_4 to CoO and this is in agreement with that obtained from experimental data using Gpf (27%). This shows that during the first step of reduction, Co_3O_4 is completely reduced to CoO. It is expected that the second step of reduction would account for 75% of the total Co_3O_4 reduced if it was completely reduced but experimental data reveals that only about 50% is reduced. It is thus concluded that Co_3O_4 is not completely reduced due incomplete reduction during the second step of reduction regardless of heating rate and reduction temperature used. Further the total extent of reduction obtained from the fitted Gpf profiles is lower (78.5%) than that obtained from the experimental TPR profile (84.5%) because the reduction due to TiO_2 support is not included.

To evaluate the amount of catalyst converted (α) at each temperature, the TPR Cobalt profile shown in Figure 5.5 was considered.

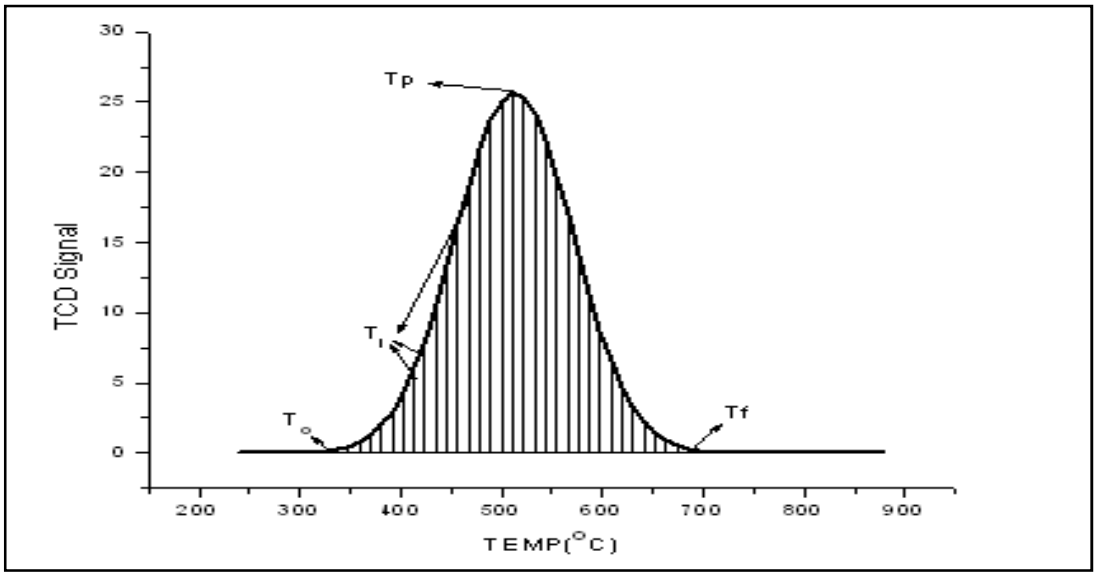

Figure 5.5 *Evaluation of TPR profile*

The area under the TPR profile between limits T_o and T_f gives the total amount of hydrogen consumed, and subsequently the total amount of catalyst converted (α). Therefore conversion at any temperature T_i along the profile can be calculated by evaluating the ratio of the integrated area between T_o and T_i to that of the total integrated area under the profile. The amount of catalyst converted (α) at any temperature is expressed as equation 5.4.

$$\alpha = \frac{\int_{Ti}^{To} \frac{d\alpha}{dT}}{\int_{Tf}^{To} \frac{d\alpha}{dT}} \quad \text{.....5.4}$$

Using equation 5.4 we can now evaluate how α changes with an increasing temperature and can help determine the general mechanism of the reduction. The α-T curves of reduction of Co/TiO_2 catalyst obtained from TPR profiles are shown in Figure 5.6 (a, b).

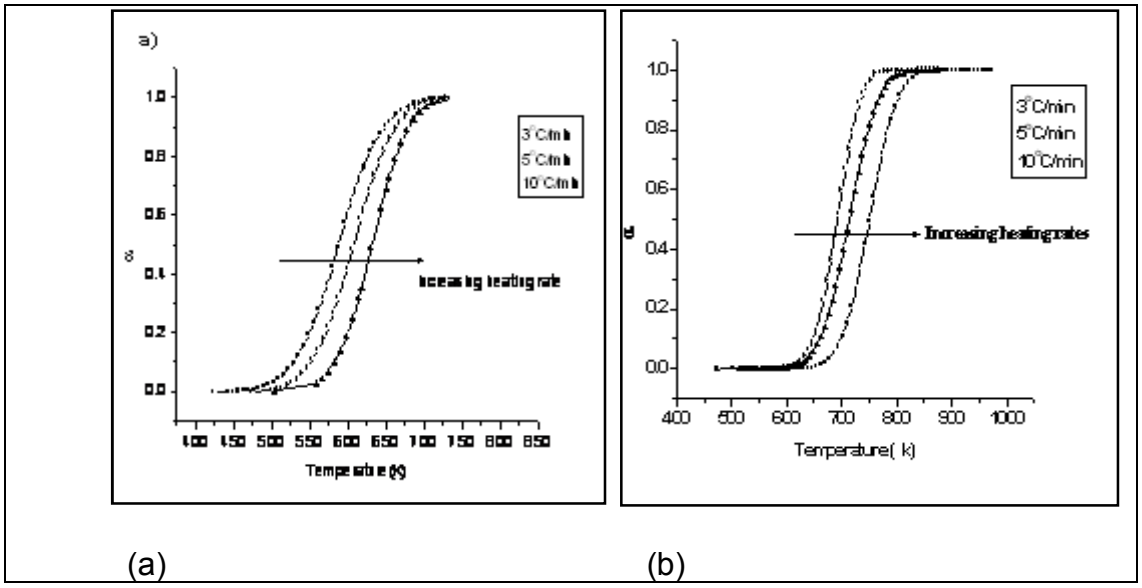

(a) (b)

Figure 5.6 *The degree of conversion (α) as a function of temperature (T) for the reduction of Co/TiO_2 catalyst under linearly rising temperature in hydrogen atmosphere at various heating rates; 3, 5 and 10 ^{o}C/min for (a) $Co_3O_4 \rightarrow CoO$ and (b) $CoO \rightarrow Co$*

The sigmoid-shaped α-T curves show the noticeable dependence of the degree of conversion on the heating rate. The reaction occurs at lower temperatures when a lower flow rate is used than when a higher ramping rate is employed.

The shapes of the α-T curve are a characteristic of the nucleation model, where the shape is sigmoid.

From the α-T curves in Figure 5.6 the rate reduction for each heating rate was evaluated, that is dα/dt = β * dα/dT, where dα/dT is the slope at any point of the curve of α versus temperature, and β is the heating rate.

The reduction rate is dependent on the heating rate employed during reduction (see Figure 5.7).

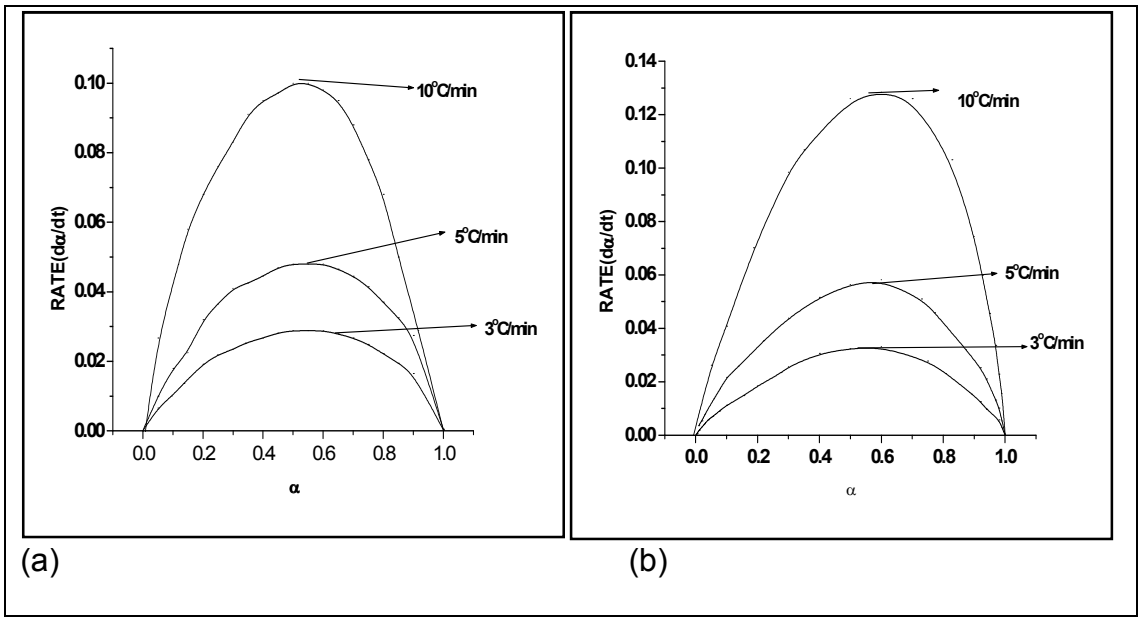

Figure 5.7 *Rate of reduction versus alpha (α) for the reduction of Co/TiO_2 catalyst at different heating rates (3, 5, and 15°C/min) for (a) Co_3O_4 →CoO and (b) CoO →Co*

The information derived from Figures 5.6 and 5.7 can be used to determine the rate of reduction at each stage of conversion with respect to

temperatures. After this the amount of H_2 consumed, and hence water produced, can be evaluated at each stage of reduction.

Table 5.3 shows the dependence of the rate of reduction (at the maximum) on the temperature at the considered heating rates based on Figures 5.6 and 5.7.

Table 5.3 Dependence of the rate of reduction (at the maximum) on the temperature at considered heating rates

β (°C/mim)	***α_{max}***	***Rate (moles.min^{-1} .gcat^{-1})***	***Temp (K)***
1st peak			
3	0.5	0.02	583
5	0.5	0.04	606
10	0.5	0.1	625
2nd peak			
3	0.6	0.02	693
5	0.6	0.06	715
10	0.6	0.12	753

The rate of reduction increases with the heating rate, and the amount of H_2 consumed is greater at a higher heating rate for both steps of reduction. This implies that at a higher ramping rate the catalyst is reduced more rapidly and reaches a limiting extent of reduction at higher temperatures. (The same observation was made in section 4.2.)

For all heating rate curves, reduction rates versus α exhibit the same shape, which suggests the same reaction mechanism and shows the dependence on the heating rate (β).

In Figure 5.8 one can see that the rates of reduction for fixed conversions at a specified temperature for a range of heating rates give the activation energy of reduction (Friedman method). As dα/dt can be difficult to measure accurately, whilst heating rate is much easier to determine, one usually prefers to plot Ln (β*dα/dt) vs 1/T. Activation energies are determined from the slopes at each conversion, as shown in Figure 5.8, where the Friedman method was applied in the conversion range of $0.2 < \alpha \leq 0.8$ for both the first and second peak. The activation energy for the two reduction steps of Co_3O_4 obtained by Friedman's method is about 81–92 $kJmol^{-1}$ for reduction degrees of the first peak, and 64–71 $kJmol^{-1}$ for the second.

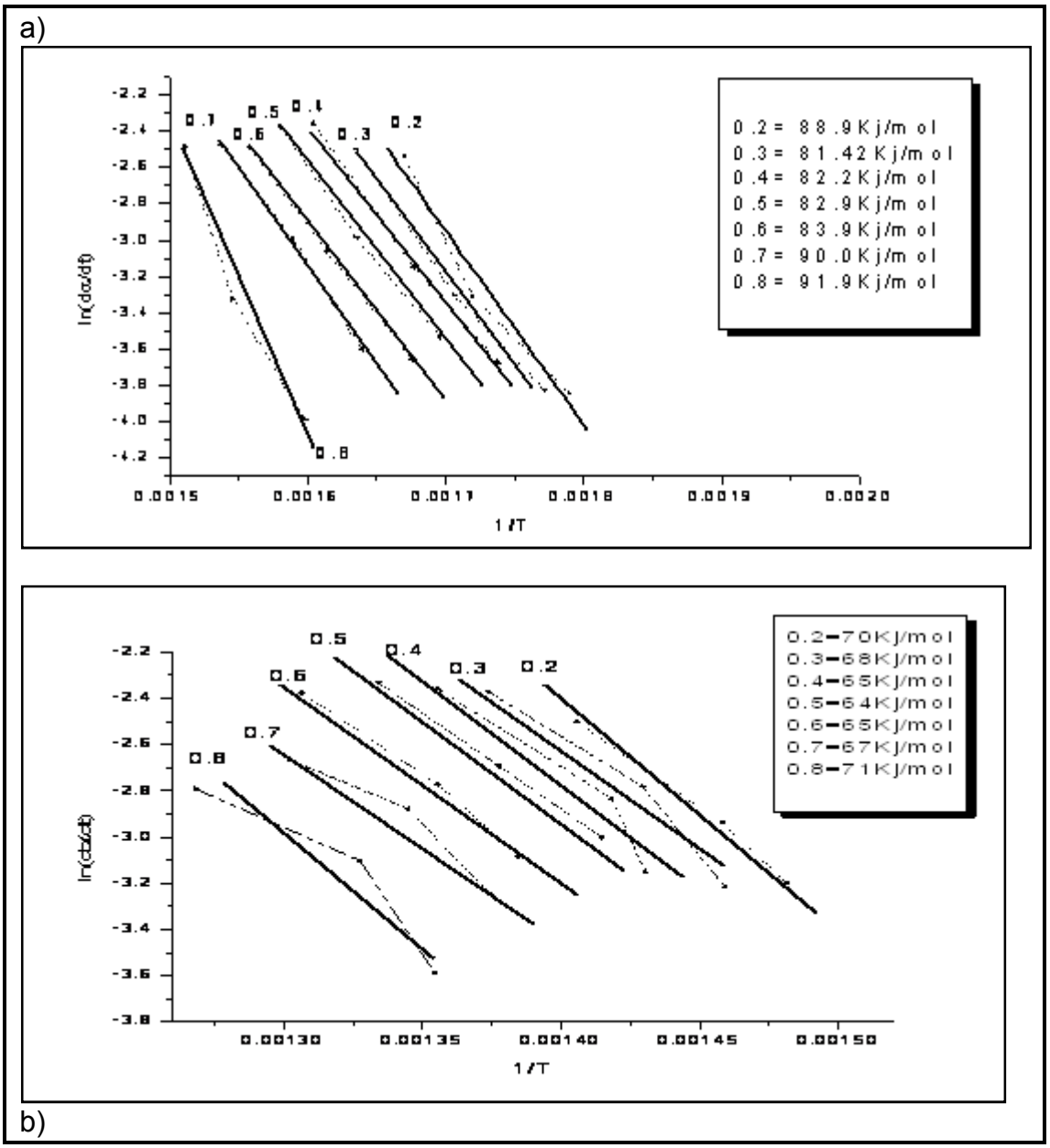

Figure 5.8 *Friedman plots generated for values of constant conversion α for (a) Co_3O_4 →CoO and (b) CoO→Co*

Analysis of the first peak

The average activation energy obtained was used for TPR kinetic modelling by application of Málek's method. (Details of the choice of reduction models based on this method are given in Appendix 4.) The functions y (α) and z (α) for the first reduction profiles were obtained by applying equations (2.16) and (2.17). The y (α) function is concave, as shown in Figure 5.9 (a). In Figure 5.9 (b) the maxima for z (α) is $\alpha_p^{\infty} \geq 0.6$. The most probable kinetic model is therefore, the avraami nucleation model (n<1) model, expressed in a generalized form as :(Sestak et al., 1984)

$$f(\alpha) = n(1-\alpha)[-\ln(1-\alpha)]^{1-1/n} \quad \text{.....5.5}$$

The n exponent is described as n = β+λ, where β is the number of steps involved in nucleus formation, and λ is the number of dimensions in which the nuclei grow. The Avraami nucleation theory is based on three main assumptions: an infinite volume *V* available for transformation; random nucleation; and the growth of transformed regions without preference of direction.

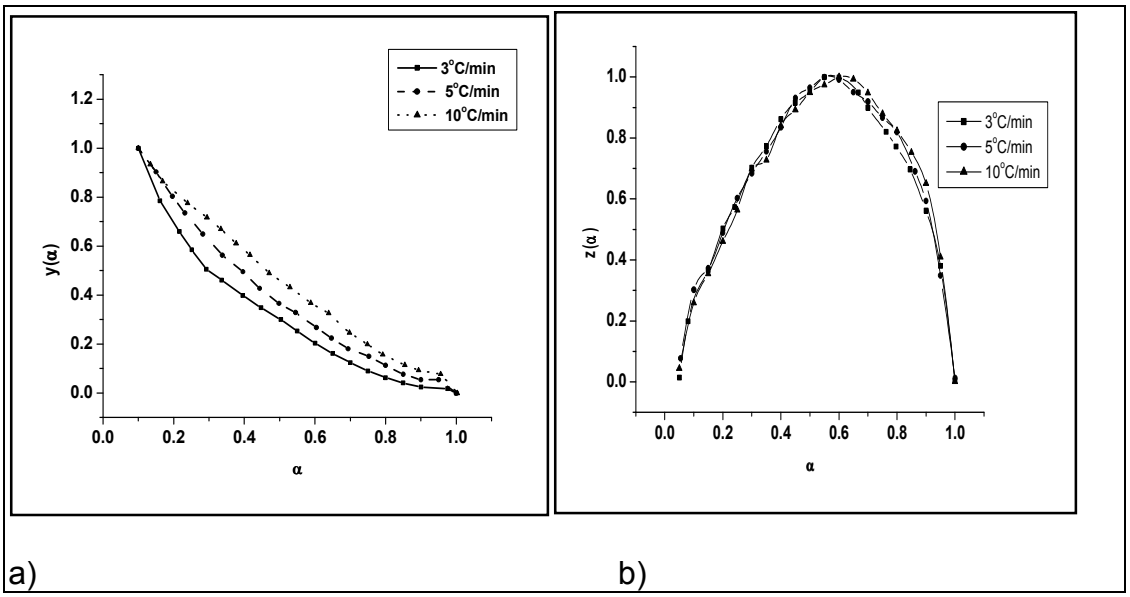

Figure 5.9 *Normalized (a) y(α) and (b) z (α) profiles for the first peak of Co /TiO_2 reduction (Co_3O_4→CoO)*

The y (α) decreases steadily, that is, n ≤ 1. The parameter n can be calculated by the Satava method (Satava, V., 1971):

ln[-ln(1-α)]= constant – n E/RT…… 5.6

The kinetic exponent n is calculated from the slope of the plot of ln [-ln (1-α)] versus 1/T.

An alternative method for calculation of the exponent n is equation 5.7 (Málek, 1992):

$$n = \frac{1-x_p\,\pi(x_p)}{ln(1-\alpha_p)+1}$$ 5.7,

where x_p is the value of E/RT at the maximum of the TA curve, and α_p is the degree of conversion maximum of the TA curve.

The pre-exponential factor A is evaluated using equation (2.16) in Chapter 2. Table 5.4 shows the kinetic parameters evaluated for the first step of reduction.

Table 5.4 Kinetic parameters evaluated for the 1st step of reduction for Co/TiO_2 catalyst (Co_3O_4→CoO)

β	***α_m***	***α_p^{∞}***	***n (Satava method)***	***A(min-1)***
3	0.1	0.6	0.49	$9.2*10^6$
5	0.1	0.6	0.59	$11.4*10^6$
10	0.1	0.6	0.60	$7.6*10^6$
Average		0.6	0.6	$9.4*10^6$

The average kinetic parameters describing the first step of reduction are E = 86 kJ/mol, ln A=16.03(min^{-1}) and n = 0.6.

The model implies that the formation of CoO nuclei at the surface of the particles is the difficult step. Once these nuclei have formed they provide sites where molecular hydrogen dissociates to yield atomic hydrogen, which promotes further reduction.

Analysis of the second peak

The average activation energy obtained (71kJ/mol) was used for TPR kinetic modelling by applying Málek's method. The y (α) and z (α) profiles for the second step of reduction were obtained by applying equations (2.10) and (2.11).

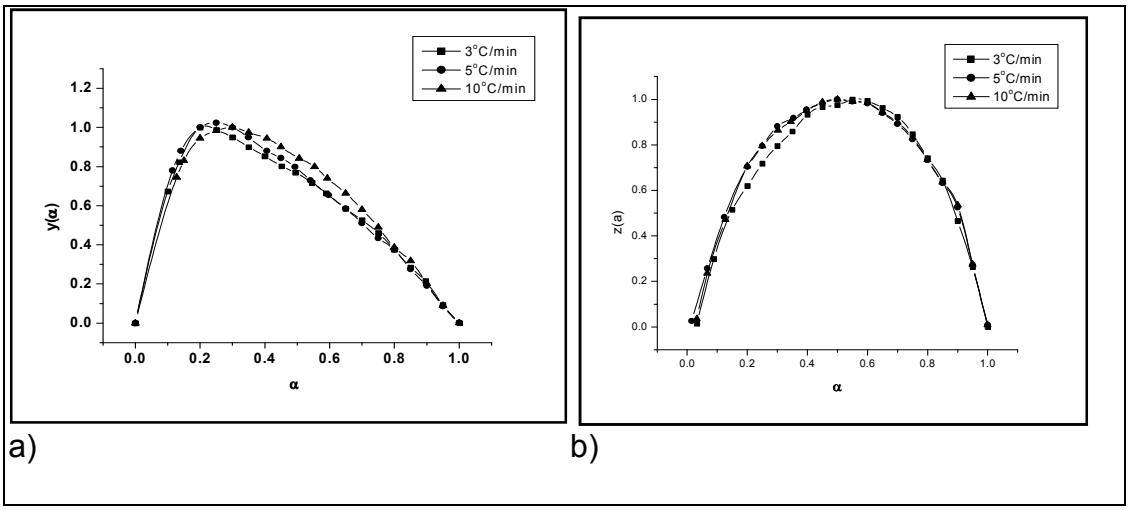

Figure 5.10 *Normalized (a) y (α) and (b) z (α) profiles for the second step of Co /TiO_2 reduction (CoO →Co)*

The shapes of the of y (α) and z (α) for various heating rates are similar (see Figure 5.10). However, the α_m and α_p^{∞} vary with the heating rates (Table 5.5).

Table 5.5 The values of α_m and α_p^{∞} of the y (α) and z (α) functions for the second step of reduction

β ***(°C/min)***	α_m	α_p^{∞}
3	0.19	0.5
5	0.29	0.5
10	0.2	0.5

The maxima of the y (α) fall into the range of $0.19 \leq \alpha_m \leq 0.29$ and $0.4 \leq \alpha_p^{\infty} \leq 0.5$ for the z (α) function. The empirical Sestak–Berggren (SB) model gives the best description if $\alpha_p^{\infty} << 0.632$ and $\alpha_m \in (0, \alpha_p)$.

It can be seen from Figure 5.10 (b) that the curve exhibits a maximum. This implies that the second reduction step occurs by a reaction mechanism similar to the nucleation and growth process described by the Avrami–Erofeev equation (r >1). However, the data could not be fitted with this equation because it assumes ideal conditions that cannot be replicated in the case of real samples. For this reason the more flexible, convenient and

empirical SB model, which gives a quantitative description of reactions that are complex or which deviate from ideal cases, was used to describe the second step of reduction.

The SB model has two parameters (m, n), as expressed in equation 5.8. If the testing method reveals that the avraami model cannot be applied, for instance if there is a considerable overlap in the nucleation and growth processes, then the two parametric SB empirical equations can be used for a quantitative description of the overall reduction.

It is shown (Málek, J., 1989) that the values of exponent m should be confined to the range 0 < m < 1: therefore

$f(\alpha) = \alpha^m (1-\alpha)^n$ ..... 5.8.

The kinetic exponents for the SB model were evaluated using Málek's procedure.

The parameter ratio of the exponents s = m/n was calculated from the maxima of the y (α) function (Málek, J., 1992), as expressed in equation 5.9:

$$s = \frac{m}{n} = \frac{\alpha_{max}}{1-\alpha_{max}} \text{.....5.9.}$$

Once the value of s (ratio m/n) is known, the values of the exponents (m and n) can be obtained using the following equation (Málek, 1992; Málek et al., 1995)

$$ln\left(\frac{d\alpha}{dt}exp\left(\frac{E}{RT}\right)\right) = ln\,A + n\,ln\left[\alpha^{s}\,(1-\alpha)\right] \quad \text{.....5.10.}$$

The exponent n corresponds to the slope of ln [(dα/dt) exp (E/RT)] versus ln [α^s (1-α)]. The value of this exponent can thus be evaluated from m = s * n. The pre-exponential factor A and the kinetic exponents m and n for each heating rate can then be determined.

Table 5.6 Kinetic parameters evaluated for the 2nd step of reduction f Co/TiO_2 catalyst (CoO→Co)

β	***s***	***m***	***n***	***lnA***
3	0.25	0.24	0.98	9.7
5	0.42	0.42	1	10.2
10	0.23	0.23	0.92	10.73
Average	*0.3*	*0.3*	*0.97*	*10.2*

The average kinetic parameters describing the second step of reduction are E = 67.1 kJ/mol, ln A=10.2 (min^{-1}) and f (α) = $\alpha^{0.3}$ $(1-\alpha)^{0.97}$

The simulated profiles for the first and second peaks at different heating rates are shown in Figure 5.11.

(a) (b)

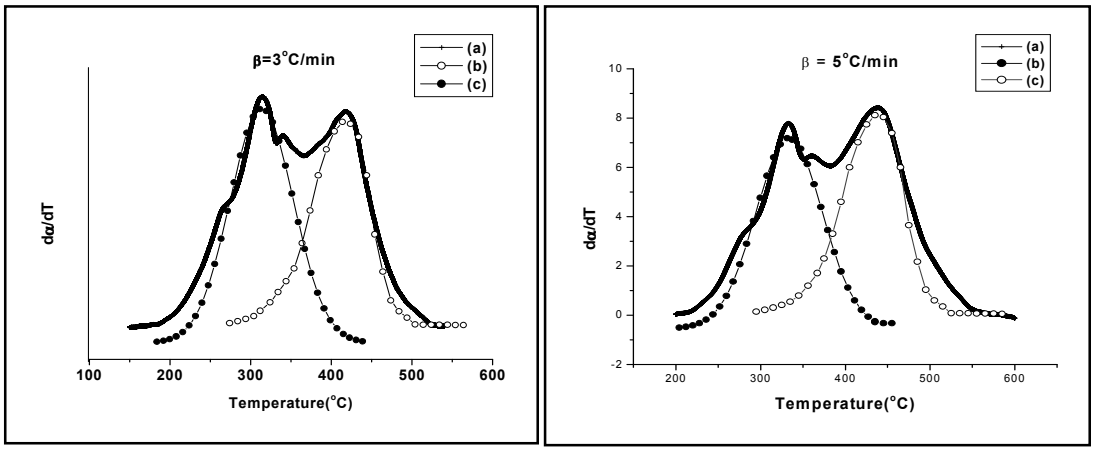

(c)

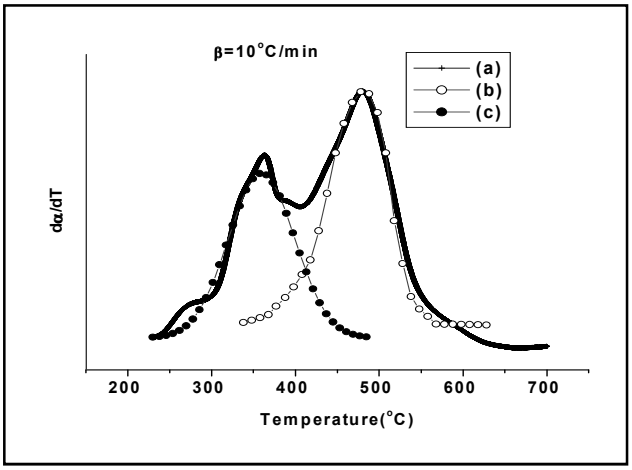

Figure 5.11 *TPR pattern of different heating rates compared with calculated data (a) experimental data; (b) simulation result of the second calculated by the Šesták– Berggren model (c) simulation result of the first peak calculated by Avrami model;*

5.4. IMPLICATIONS AND APPLICATIONS FOR A 12 M LONG TUBE

Information obtained from kinetic analysis using TPR can be used to determine the dependence of the rate of reduction on temperature. Using the resultant findings, the rate of reduction can be evaluated at each stage of conversion for a particular heating rate, which in turn will help determine the optimum temperature for reduction without overheating the catalyst. An optimum heating rate that allows the gradual reduction of the catalyst, which results in gradual production of water at relative temperatures, can then be selected. The temperatures at which different stages of reduction occur can also be evaluated to predict the temperatures at which P_{H_2O} will be expected to increase or decrease in a 12m long tube during reduction. This would improve the control and monitoring of P_{H_2O}.

The mechanism of reduction obtained from kinetic analysis can help explain the degree of reduction observed as a function of time for various temperatures. Because it gives greater understanding of the stages of reduction and the underlying gas solid reactions, the findings obtained through the analysis can be used as a guide to monitor and control P_{H_2} in a 12m long tube throughout the reduction process.

5.5 REFERENCES

1. Armouldy, P. and Moulijn, J.A (1985), *Journal of Catalysis*, 93, 38.
2. Friedman, H. L., (1963), *Journal of Polymer Science Part C 6*, 183–195.
3. Hurst, N.W., Gentry, S.J., Jones, A. and McNicol, B. D. (1982), *Catalysis Reviews – Science and Engineering*, 24, 33.
4. Jones, A. and McNicol, B. D. (1986), Marcel Dekker, New York, 199.
5. Kissinger, H. E. (1957), *Analytical Chemisry*, 29, 1702.
6. Knözinger, H., Ertl, G. and Weitkamp, J. (1997), *Handbook of Heterogeneous Catalysis*; Eds.; VCH.
7. Malet, P. and Caballero, A. (1988) A. *Journal of the Chemical Society*, *Faraday Transactions,* 84, 2369.
8. Málek , J. (1989), *Thermochim. Acta*, 138, 337.
9. Monti, D.A. M. and Baiker, A. (1983), *Journal of Catalysis*, 83, 323.
10. Niemantsverdriet J. W., *Spectroscopy in Catalysis: An Introduction*, Edittion 3, 2007, Eindhoven University of Technology, the Netherlands.
11. Robertson, S.D., McNicol, B.D., De Baas, J. H., Kloet S. C. and Jenkins, J.W. (1975), *Journal of Catalysis*, 37, 424-431.
12. Satava V., (1971) *Thermochim. Acta*, 2, 423.

13. Sestak, J., Satava V., Wendlandt, W. W. (1973), *Thermochim. Acta*, 7 333-556.
14. Sexton, B.A., Hughes, A.E, and Turrney, T.W. (1986), *Journal of Catalysis*, 97, 390.
15. Tafoui, A. (1996), Phd thesis, Delft University of Techchnology, The Netherlands.
16. Wimmers, O.J, Arnoldy, P., and Moulijn, J.A. (1986), *Journal of Physical Chemistry*, 90, 1331-1337.

CHAPTER 6

CONCLUSIONS AND RECOMMENDATIONS

The main objectives of this study were to: (1) use TPR quantitative and qualitative information based on the relevant literature, and on assumptions and experimental data to help understand the implications of reduction conditions on catalyst in a 12 m long tube in industry; (2) to evaluate the effects of different conditions during catalyst reduction, for application in the design of better reduction procedures and an improved comparative understanding of real operating conditions; and (3) to develop and apply methods of kinetic analysis and models for use in a basic kinetic evaluation of catalyst reduction reactions involving multi-step reduction processes. The conclusions and recommendations made on the basis of the work to fulfil objectives are stated below.

1) It has been shown that mass balance calculations based on the TPR system can be used to generate reduction flow sheets that can be used to determine reduction conditions in a 12 m long tube. However,

it is recommended that certain amendments relating to the different conditions in the two systems (that is reduction using TPR and that in a large scale reactor), for example operating temperatures and pressures, support reducibility, P_{H_2O} and the partial pressures of the reducing gas, be made when undertaking comparative calculations. Alternatively, for a more realistic approach and better prediction of P_{H_2O}, TPR can be modified to run at conditions similar to those in a 12 m long tube. This can be used to make a more accurate determination of P_{H_2O} before reduction of catalyst on a large scale by means of a kinetic model.

Using information elicited from the scientific literature and experimental data, it has been found that P_{H_2O} prior to and during reduction has an effect on catalyst reducibility. On the other hand, the amount of water present in the catalyst before reduction (depending on extent of atmospheric exposure) and that produced during reduction of the bulk catalyst in a 12 m long tube would relatively be substantial and TPR provides an indication of the effects.

It is also recommended that since the close monitoring of P_{H_2O} and P_{H_2} in a 12 m long tube may not be sufficient to eliminate the problem of

P_{H_2O} during reduction, a means of removing water, for instance absorption, should be investigated in the future.

2) Among the parameters investigated, heating rate and drying time prior to reduction were found to have a significant impact on catalyst reducibility. It was established that a lower ramping rate maximizes the extent of reduction to active Co metal at relatively low temperatures, while at the same time ensuring an equilibrium particle size that is stable against sintering. It was observed that water in the catalyst prior to reduction had a significant effect on catalyst reducibility. However, this is contrary to what would be expected, as a higher degree of reduction would be expected on the crushed catalyst rather than on the uncrushed catalyst because of the larger catalyst surface area available on the former. Therefore, no conclusive explanation could be made. It was thus recommended that FT experiments should be performed on the catalyst with varying degrees of water content so as to investigate the effect based not only on the reducibility of the catalyst but also on its activity and selectivity.

3) It has been shown that kinetic analysis using TPR can be used to determine the optimum reduction temperature. The temperatures at which different stages of reduction occur (in the case of multi-step

reduction) can be evaluated and used to predict the amount of H_2 that will be consumed as the temperatures increase, which is helpful when used in monitoring and controlling P_{H_2O} in a 12 m long tube.

Furthermore, the mechanism of reduction obtained from kinetic analysis can help understand the degree of reduction observed as a function of time for various temperatures. It also helps understand the stages and underlying gas solid reactions hence can be used as a guide to monitor and control P_{H_2} throughout the reduction process in a 12m long tube.

APPENDIX 1

TPR CONTROLLER OPTIMIZATION

A proportional-integral-derivative (PID) controller, as shown in Figure A1, was used to correct the error between a measured temperature and a desired (set) temperature by calculating and then indicating (outputting) what corrective adjustment should be made.

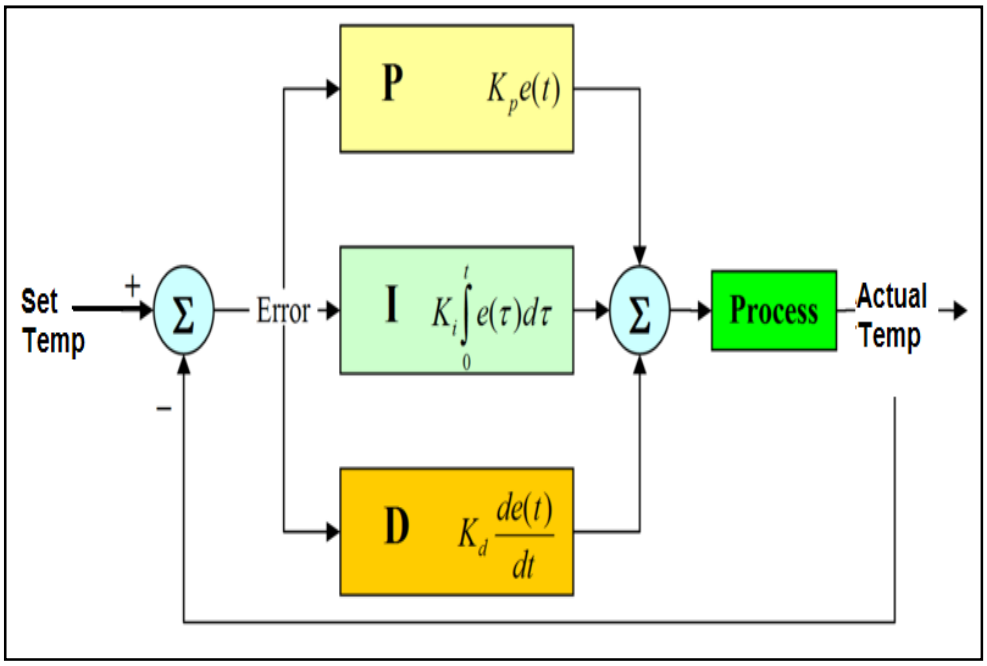

Figure A1 *PID controller*

1. Proportional value

The proportional term makes a change to the output that is proportional to the current error value. Typically this is the main drive in a control loop, and reduces a large part of the overall error.

2. Integral value

The contribution of the integral term is proportional to both the magnitude of the error and its duration. It reduces the final margin of error in a system.

3 Derivative value

The derivative value determines the rate at which the error changes, by slowing the rate of change in the controller output. This effect is most noticeable close to the controller's set point. Hence, derivative control is used to reduce the magnitude of the overshoot produced by the integral component, and to improve the stability of the controller–process combination. However, the differentiation of a signal amplifies the noise it makes.

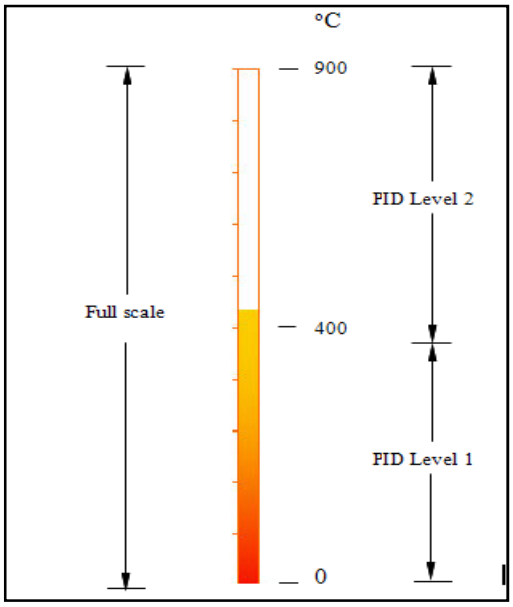

Figure A2 Level PID

This term in the controller is highly sensitive to noise in the error term, so if the noise and the derivative gain are sufficiently great they can cause a process to become unstable.

The weighted sum of these three values was used to adjust the process via the power supply of the heating element in the furnace. Initially only one level (that is, only one range of temperature; 0°C–900 °C of PID) was used to optimize the controller. However it was observed that there was a large temperature lag, especially at higher temperatures.

The level PID function was used to set PID control constants individually, by dividing the full scale into two levels (0–400 ^{o}C and 400–900 ^{o}C), as shown in Figure A2, in order to achieve finer temperature control. This is critical in TPR kinetics because the interpretation of the rate of reduction is greatly influenced by differences between measured and set temperatures.

APPENDIX 2

MASS BALANCE CALCULATIONS

The manufacturers' specifications provided details on the.composition of the feed gas.

Molar flow rate into the reactor was calculated by:

= (% hydrogen in) x (volumetric flowrate /22400)

= (5/100 x 5 x 10^-3/22.4)mol/min

= 1.12 x 10^-5 mol/min

So 1.12^-5 mol of hydrogen passes through the reactor every minute when a flow rate of 5ml/min is used. Table A1 shows different molar flow rates when various flow rates (5, 10, 15, 30ml/min) of 5% H_2 are used.

Table A1 Molar flow rate for various flow rates

Flow rate of gas mixture into the reactor (cc/min)	***% H_2 in carrier gas***	***Molar flowrate of H_2 (mol/min)***
5	5	1.12x10^-5
10	5	2.23 x10^-5
15	5	3.34 x10^-5
30	5	6.69 x10^-5

The amount of hydrogen gas required for the complete reduction of Co_3O_4 to metallic cobalt was calculated according to the equation:

$Co_3O_4 + 4\ H_2 \rightarrow 3\ Co + 4\ H_2O$ ……1

241g 8g

The mass of the catalyst used in the analysis when 10% of Co by wt was used in the preparation of the catalyst:

= 10/100 x 0.015g

=1.5 x 10^{-3} g of Co is present in the 0.015g sample.

Thus the total amount of hydrogen gas required for the complete reduction of Co_3O_4 to metallic cobalt was:

= $(1.5x10^{-3} \times 8) / (241 \times 2)$

= $\underline{2.97 \times 10^{-5} \text{ moles.}}$

The total time taken for the completion of the reactions at different flow rates is summarized in Table A2.

Table A2 Effect of heating rate on time required for complete reduction

Heating Rate (^oC/min)	***Total time (min)***	***Total hydrogen supplied(moles) during reduction***	***Total hydrogen consumed(moles)***
3	133	1.49×10^{-3}	2.97×10^{-5}
5	70	7.84×10^{-3}	2.97×10^{-5}
10	65	7.28×10^{-4}	2.97×10^{-5}

The supply of hydrogen is constant, so the total amount of hydrogen supplied at the end of reduction for all three runs will be much greater than the amount of hydrogen consumed in the complete reduction. The total amount of H_2 supplied is about 50 times more than that consumed when a 3^oC/min heating

rate is used, and 24 times greater at a 10^{o}C/min rate. This shows that the flow rate of the reducing gas mixture employed is reasonable, and that no instantaneous depletion of H_2 will occur, even when the rate of reduction is increased.

APPENDIX 3

EXPERIMENTAL PRECAUTIONS

TPR is very sensitive, and therefore is easily affected by various factors. To obtain reproducible results that can be used for kinetic or other kinds of analysis, certain precautions have to be taken, among them the following.

1. Optimization of PID

Before any runs are performed, the PID controller has to be calibrated and optimized so that there are no differences between the set temperature and actual temperature

2. TPR reactor position

The position of the reactor in the furnace should be constant for all runs performed. Changing the position of the reactor in the furnace will give different onset temperatures of reduction. Although the differences are not significant, this is an important precaution when TPR is used for kinetic analysis.

3. External factors

Because TPR is very sensitive to noise, the profiles can be altered by the movement the equipment while thermo grams are being recorded. The equipment should therefore be placed in a stationary position.

Room temperature and pressure also affect TPR profiles, so these potential sources of interference should be taken into account at the start of each run.

4. Heat losses

When heat is lost from the furnace, this can result in a lag between the set and the measured temperatures. This can be avoided by lagging the furnace, especially at the top, where it is open. Depending on the room's ventilation system, one can also keep the doors and windows closed.

APPENDIX 4

MÁLEK'S METHOD OF MODEL SELECTION

After the activation energy has been calculated, the kinetic model which best describes the set of thermal analysis data can be obtained. For this purpose, two special functions y (α) and z (α), which are obtained by transformation of experimental data (Málek, J., 1989; Criado et al 1989) are defined:

$y(\alpha) = (d\alpha/dt)\, exp\, (x)$……....1

$z(\alpha) = \pi(x)\, (d\alpha/dt)\, T/\beta$…….....2

where x=E/RT and π (x) is an approximation of the temperature integral. The rational expression of Senum and Yang (1977) is used to estimate π (x):

$$\pi\,(x) = \frac{x^3 + 18x^2 + 88x + 96}{x^4 + 20x^3 + 120x^2 + 240x + 120}$$ ……3.

The y (α) function is proportional to the f (α) function. Thus, by plotting the y (α) dependence normalized within the (0, 1) interval, the shape of the function

f (α) is obtained. The y (α) function is therefore a diagnostic tool for kinetic model determination. The maximum alpha α_m for the y (α) and α^{∞}_{p} for the z (α) function are used to guide the choice of a kinetic model (Málek, J., 1989).

Determination of the maxima of z (α) function (α^{∞}_{p})

An alternative expression of the reaction rate can be obtained by combining equations 1 and 2:

$d\alpha/dt = Ae^{-x} f(x)$……4

$g(\alpha) = \int_0^{\alpha} \frac{d\alpha}{f(\alpha)} = exp^{-x}[\frac{\pi(x)}{x}]$……5

to get equation 3:

$d\alpha/dt = [\frac{\pi(x)\left(\frac{d\alpha}{dt}\right)T}{\beta}] = f(\alpha)g(\alpha)$……6.

After rearrangement of equation 6:

$z(\alpha) = \frac{\pi(x)\left(\frac{d\alpha}{dt}\right)T}{\beta} = f(\alpha)g(\alpha)$.....7,

and differentiating the equation with respect to α:

$Z'(\alpha) = f'(\alpha)\, g(\alpha) + 1$.....8,

And by setting equation 8 equal to zero, equation 9 is obtained. This must be fulfilled by α^{∞}_{p} at the maximum of z (α):

$-f'(\alpha^{\infty}_{p})\, g(\alpha^{\infty}_{p}) = 1$.....9.

The parameter α^{∞}_{p} gives characteristic values (Criado et al, 1982) for basic kinetic models, as summarized in Table 1.The parameter α^{∞}_{p} is independent of the values of activation energy.

Table A1 The values of the parameter a α^{∞}_{p}

model	α^{∞}_{p}
JMA (n)	0.632
R2	0.750
R3	0.704
D2	0.834
D3	0.704
D4	0.776

Determination of the maximum of y (α) function

Comparing equations 4 and 1, the function y (α) can be expressed as follows:

y (α) =A f(α)……..……10

Therefore the condition for the maximum of the y(a) function can be written as f'(a)**=**0. By analyzing this condition, one can find that the D2, D3, D4 and RO (n) kinetic models have a maximum at $\alpha_m = 0$. It can also be shown that there is a maximum of the y (a) function $0 < \alpha_m < \alpha_p$ for both the JMA (n) and SB

(m, n) models, which depends on the value of the kinetic exponents. The condition for the maximum of the JMA (n > 1) model is given by the equation:

$\alpha_m = 1- exp\ (1-n/n)$……..11.

Similarly, the condition for the maximum of the SB (m, n model) is expressed by

$\alpha_m = m/m+n$……12.

Table A2 and Table A3 give f (α) functions for some gas–solid reaction models that are relevant for describing the reaction mechanism. The most frequently-used basic kinetic models are summarized in Table A2.

Table A2 Basic kinetic models

Models	***Symbol***	***f(α)***	***Properties of the y(α) function***
Johnson–Mehl–Avraami	JMA(n)	$n(1-\alpha)[-\ln(1-\alpha)]^{1-1/n}$	Concave for n<1,linear for n=1,maximum for n>1
2D-reaction	R2	$(1-\alpha)^{1/2}$	Convex
2D-reaction	R3	$(1-\alpha)^{1/3}$	Convex
2D- diffusion	D2	$1/[-\ln(1-\alpha)]$	Concave
Jander equation	D3	$3/2(1-\alpha)^{2/3}/[1-(1-\alpha)^{2/3}]$	Concave
Ginstling–Brounshtein	D4	$3/2[1-\alpha)^{-1/3}-1]$	Concave

The exponent n in the Johnson–Mehl–Avrami equation depends on the mechanism of the nucleation–growth process. In most of the cases that have been studied, the exponent n remains constant for the greater part of the reaction (Šesták et al., 1984). The y (α) function varies with different reaction models, as illustrated in Figure A1.

In addition to the basic kinetic models that correspond with certain geometries of the reaction interface, there are empirical kinetic models (see Table A3). It was shown

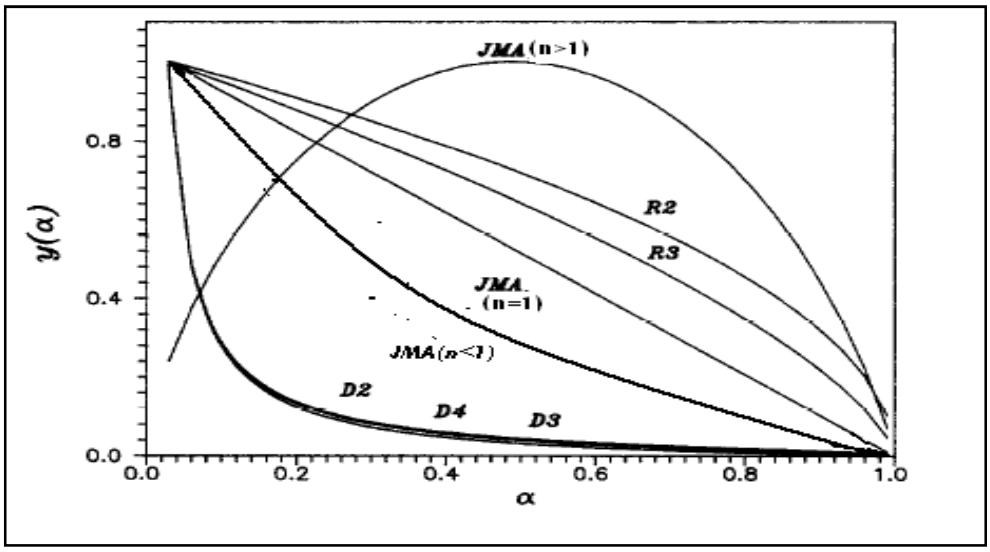

Figure A1 *Typical y (α) functions for basic kinetic models*

that acceptable values of the parameter m for SB models are confined to the interval 0<m<1 (Málek, J., 1989).

Table A3 Empirical kinetic models

Models	***Symbol***	***f (α)***
Reaction order	RO(n)	$(1-\alpha)^n$
Šesták–Berggren	SB (m,n)	$\alpha^m (1-\alpha)^n$

Combinations of the of α_m and α^{∞}_p are used to determine the most suitable kinetic model. The criteria for choosing a suitable model are summarized in Figure A2.

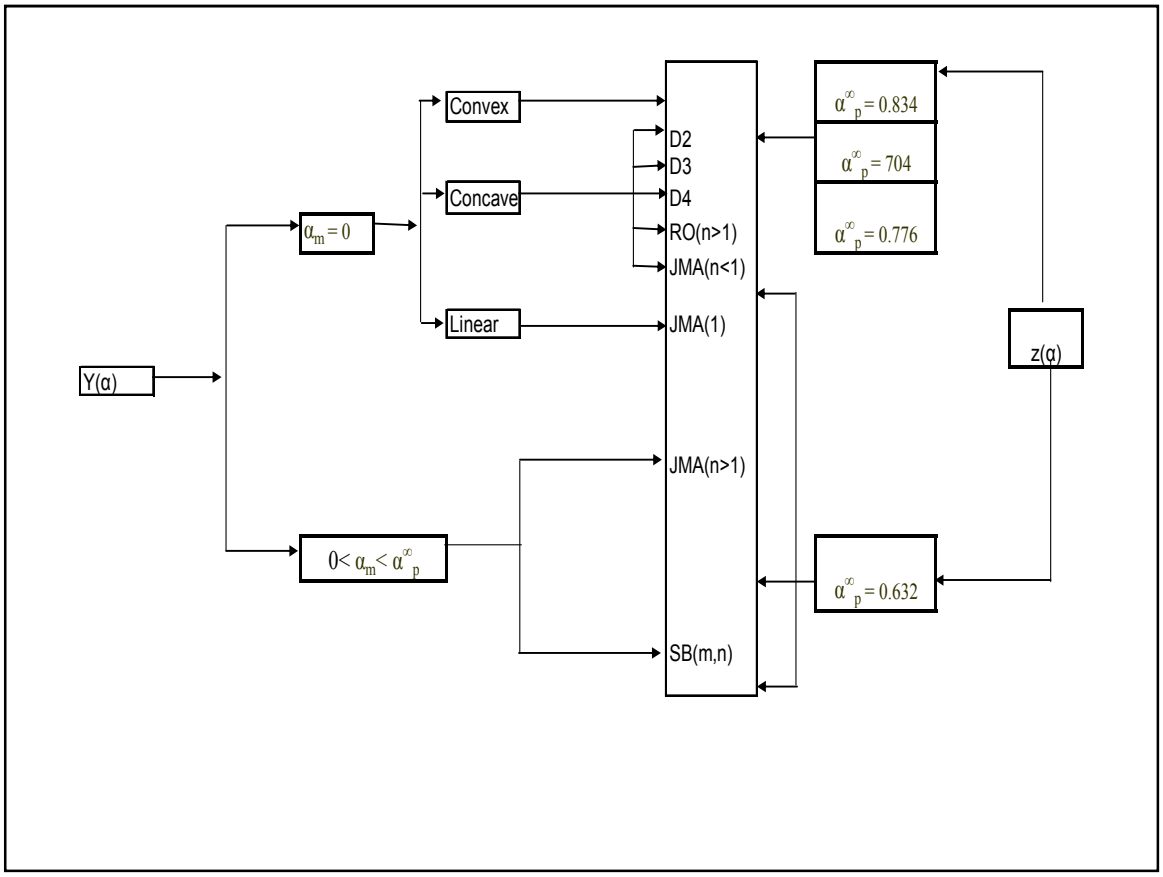

Figure A2 *Schematic diagram of kinetic model determination*

APPENDIX 5

TPR CALIBRATION

TPR apparatus was calibrated by means of a standard silver oxide (AgO) sample. AgO is used because it is completely reduced under the flow hydrogen. The reaction is given as:-

$AgO+H_2 \rightarrow Ag + H_2O$

The manufacturer's specifications provided details of standard AgO and TPR conditions that can be used i.e. ramping rate, mass of AgO and the composition of the reducing gas that would result in a given shape of the reduction profile, the amount of reducing gas consumed and the maximum peak temperature.

TPR experiments were carried out using 5% H_2/Ar (flow rate, 5, 10 and 15ml/min; pressure, 1bar) as the reducing gas and a sample mass of 15 mg. Prior to each TPR run AgO was degassed and dried under pure Argon gas at a rate of 10^{o}C/min to 150^{o}C, and then left for 20 minutes at 150^{o}C. TPR runs

were carried out after the sample had cooled to room temperature under the flow of argon. The temperature was ramped at 10^{o}C/min to 800^{o}C. .

There was a notable variation in areas under the peak for the different flow rates used and this is expected as the integrated areas depends on the concentration (ie number of mols of H_2 /cm^3) and thus the flow rate used. The total hydrogen consumed was thus evaluated by the product of the flow rate and the area under the TPR curve for each flow rate used. TPR profiles in Figure A1 shows TPR profiles at different flow rates.

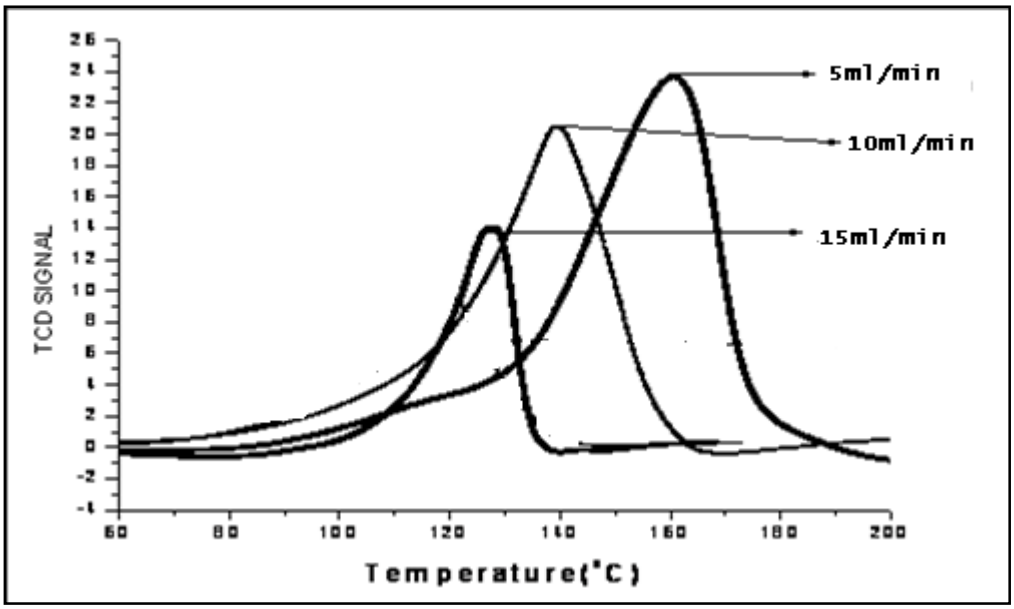

Figure A1 *TPR profiles for the reduction of AgO for catalyst at flow rates: 5, 10 and 15ml/min*

Though the area under the profiles is different the total hydrogen consumed is the same at all flow rates. Table A1 shows the variations of the areas with the flow rate.

Table A1 variations of the areas with the flow rate.

Flow rate (cc/min)	***Area under TPR profile***	***Area * Flow rate***
5	22455.4	112276.8
10	10934.7	109346.6
15	7360.1	110406.8
Average		110676.8

Based on the data in Table A1, the average area based flow rates was used to represent the total amount of H_2 that would be consumed when AgO is completely reduced. Thus using stoichiometric equations the amount of H_2 that would be consumed and the extent of reduction for the Co/TiO_2 at similar conditions was evaluated.

APPENDIX 6

PEAK SEPERATION

The Co catalyst is assumed to undergo two separate reactions ($Co_3O_4 \rightarrow CoO \rightarrow Co$) before the catalyst is completely reduced. Based on this, an attempt was made to separate the two peaks using TPR.

TPR experiments were carried out using 5% H_2/Ar (flow rate, 5ml/min; pressure, 1bar) as the reducing gas and a sample mass of 15 mg. All of the experimental conditions were in agreement with those recommended by Monti and Baiker (1983). Prior to each TPR run the catalyst was degassed and dried under pure Argon gas at a rate of 10^oC/min to 150^oC, and then left for 20 minutes at 150^oC. TPR runs were carried out after the sample had cooled to room temperature under the flow of argon. The temperature was ramped at 10^oC to various constant temperatures (320,340,360 and 380^oC) and kept constant for one hour to allow for a good baseline. After that the temperature was ramped up again to 800^oC from the respective constant temperatures. Figures A1 to A5 illustrate the variation of reduction profiles with various temperatures employed.

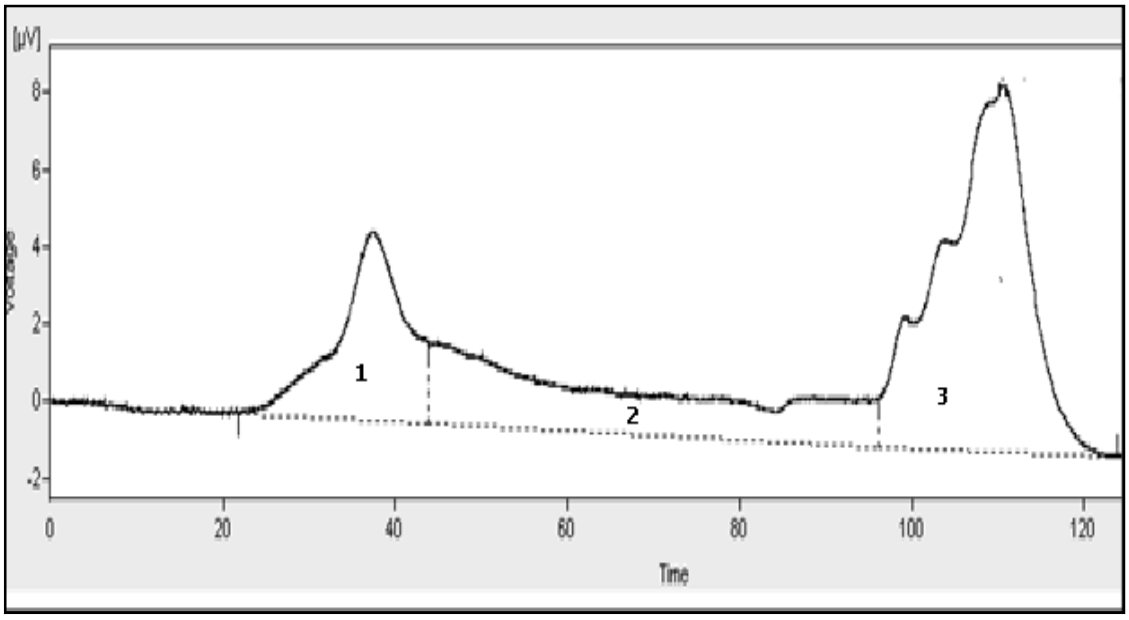

Figure A1 Constant temperature; 320^{o}C

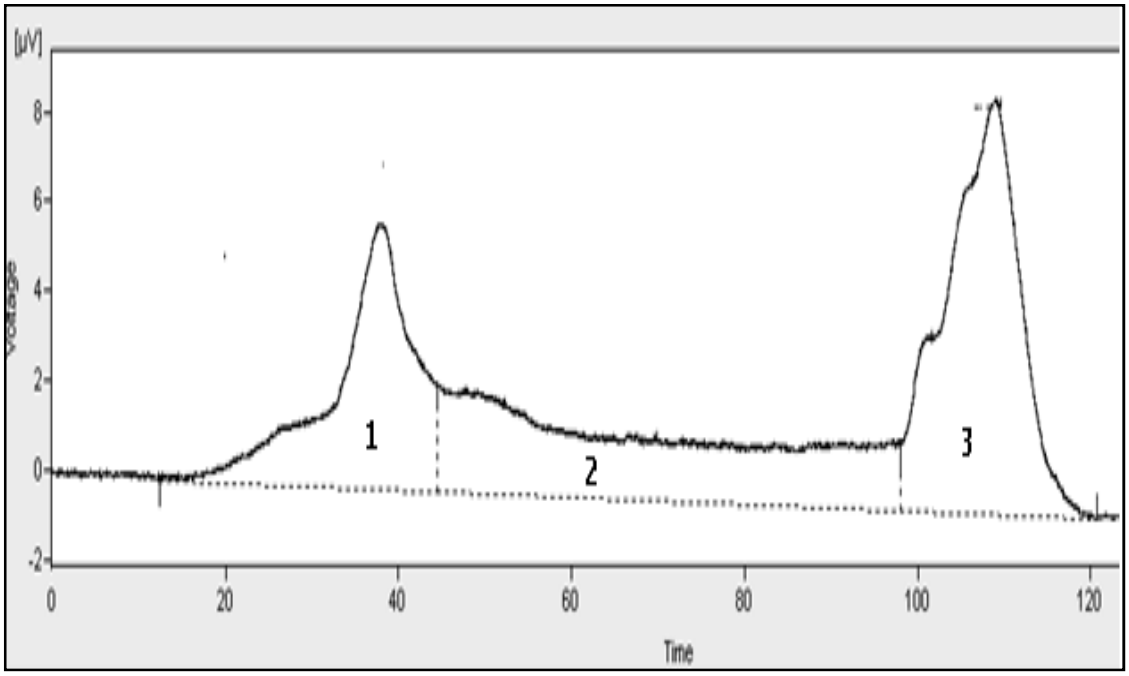

Figure A2 constant temperature; 340^{o}C/min

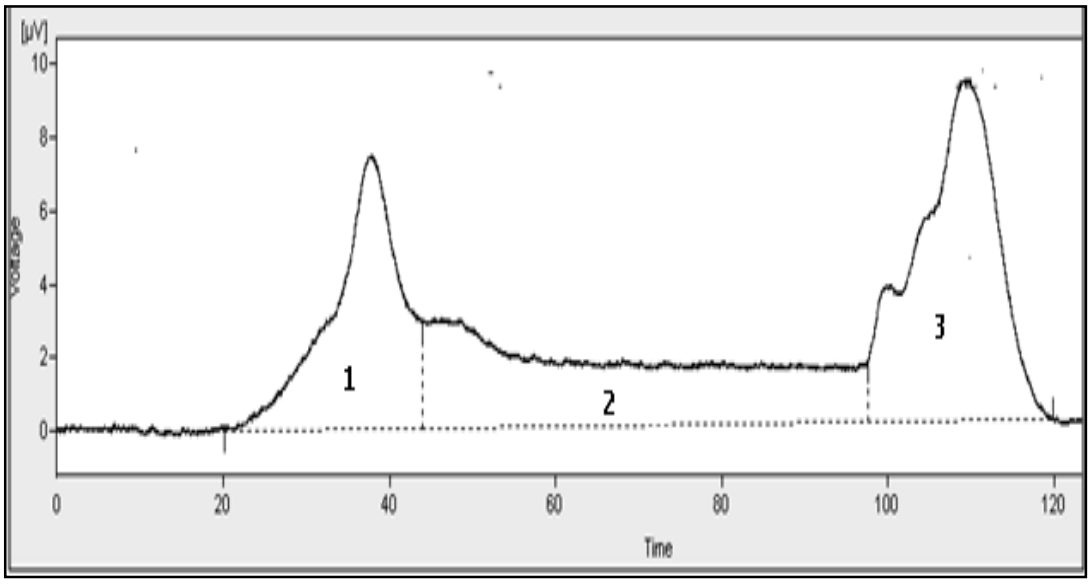

Figure A3 constant temperature; 350^{o}C

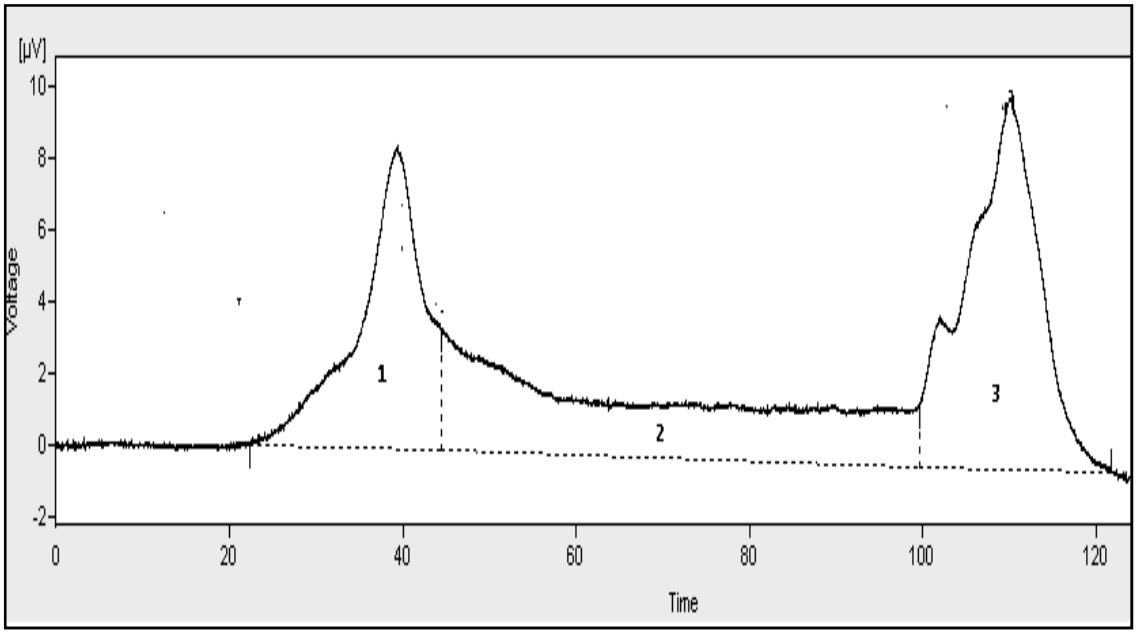

Figure A4 constant temperature -360^{o}C

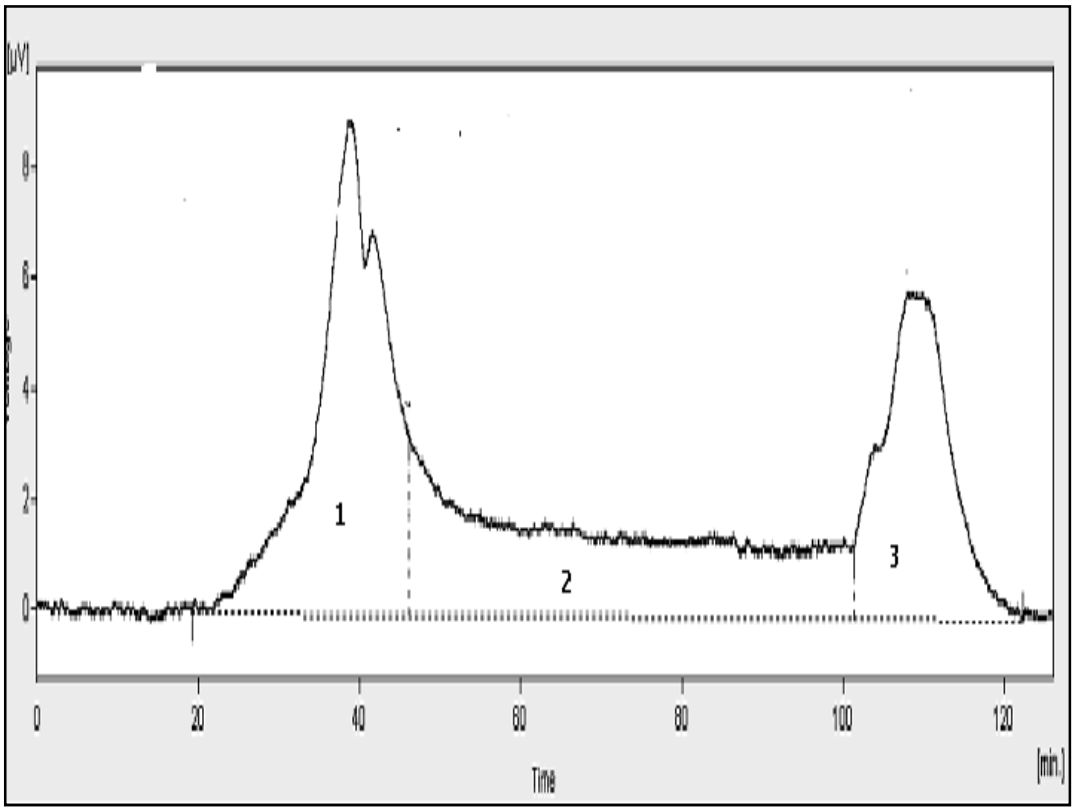

Figure A5 constant temperature; 380^{o}C

To investigate how reduction varies with temperature , the areas under the peaks at the three phases were evaluated that is ;area under the temperature profile from room temperature to constant temperature(Area1),area under the constant temperature profile (area 2) and the area under the temperature profile from constant temperature to completion(area 3).This is illustrated in Table 1.

Table A1 variation of area with constant temperatures

Constant Temp	*Area 1*	*% area*	*Area 2*	*% Area*	*Area 3*	*% Area*	*Total area*
330	2447.4	17.0	5168.0	35.9	6777.2	47.0	14392.7
340	2798.4	19.6	5272.9	36.9	6201.1	43.4	14272.4
350	3172.6	21.7	5289.3	36.2	6141.0	42.0	14603.0
350	3082.2	21.9	4910.0	34.9	6036.7	43.0	14029.1
360	4111.0	26.0	5607.4	35.5	6055.0	38.3	15773.5
380	5238.8	37.3	5198.3	37.0	3599.8	25.6	14037.0

Referring to Table A1 on the top, by plotting the total area for the three respective phases against the temperatures, the following Figure A6 is realized.

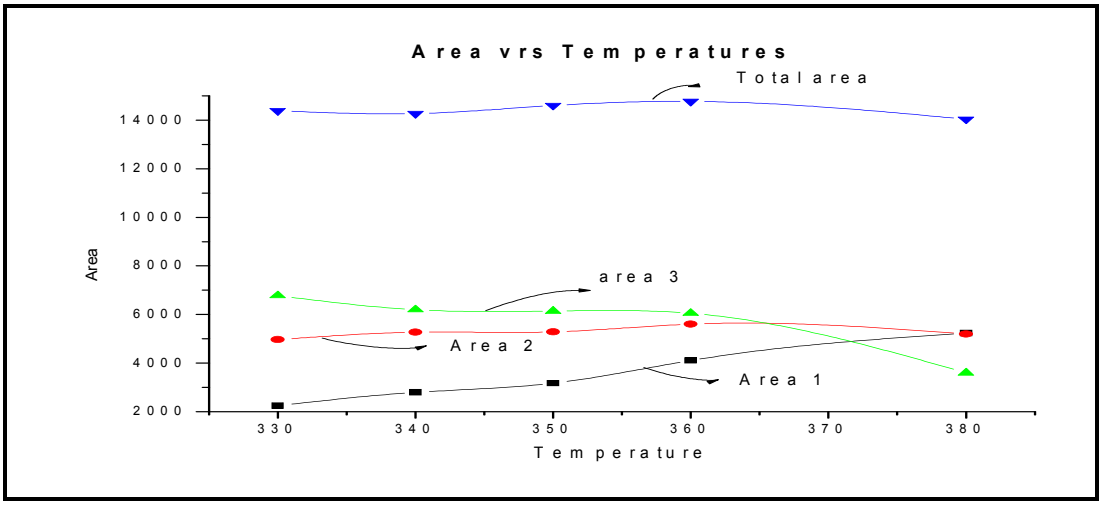

Figure A6 variation of area with constant temperatures

It is interesting to note that the total area for the various constant temperatures employed is constant which shows that the extent of reduction is no affected temperature variation during the process of reduction provided that the reaction is allowed to go to completion.

It is recommended that further work be done using this approach as it provides a good basis for kinetic evaluation of complex reduction reactions involving multi-step reduction processes.